Experimental Eye Research 132 (2015) 17–33

Contents lists available at ScienceDirect

Experimental Eye Research

journal homepage: www.elsevier.com/locate/yexer

Laser-induced ocular hypertension in adult rats does not affect non-RGC neurons in the ganglion cell layer but results in protracted severe loss of cone-photoreceptors

Arturo Ortín-Martínez [1], Manuel Salinas-Navarro [1], Francisco Manuel Nadal-Nicolás, Manuel Jiménez-López, Francisco Javier Valiente-Soriano, Diego García-Ayuso, José Manuel Bernal-Garro, Marcelino Avilés-Trigueros, Marta Agudo-Barriuso, María Paz Villegas-Pérez, Manuel Vidal-Sanz*

Departamento de Oftalmología, Facultad de Medicina, Universidad de Murcia, and Instituto Murciano de Investigación Biosanitaria Virgen de la Arrixaca (IMIB-Arrixaca), 30100 Murcia, Spain

ARTICLE INFO

Article history:
Received 21 August 2014
Received in revised form
19 November 2014
Accepted in revised form 7 January 2015
Available online 7 January 2015

Keywords:
Ocular hypertension
Adult albino rat retinal ganglion cells
Neuronal degeneration
S-cones L-cones
Photoreceptors loss
Displaced amacrine cells
Ganglion cell layer of the retina
Outer retinal layers
Elevated intraocular pressure
Limbar laser photocoagulation
Rodent experimental glaucoma model

ABSTRACT

To investigate the long-term effects of laser-photocoagulation (LP)-induced ocular hypertension (OHT) in the innermost and outermost (outer-nuclear and outer segment)-retinal layers (ORL). OHT was induced in the left eye of adult rats. To investigate the ganglion cell layer (GCL) wholemounts were examined at 1, 3 or 6 months using Brn3a-immunodetection to identify retinal ganglion cells (RGCs) and DAPI-staining to detect all nuclei in this layer. To study the effects of LP on the ORL up to 6 months, retinas were: i) fresh extracted to quantify the levels of rod-, S- and L-opsin; ii) cut in cross-sections for morphometric analysis, or; iii) prepared as wholemounts to quantify and study retinal distributions of entire populations of RGCs (retrogradely labeled with fluorogold, FG), S- and L-cones (immunolabeled). OHT resulted in wedge-like sectors with their apex on the optic disc devoid of $Brn3a^{+}$RGCs but with large numbers of $DAPI^{+}$nuclei. The levels of all opsins diminished by 2 weeks and further decreased to 20% of basal-levels by 3 months. Cross-sections revealed focal areas of ORL degeneration. RGC survival at 15 days represented approximately 28% and did not change with time, whereas the S- and L-cone populations diminished to 65% and 80%, or to 20 and 35% at 1 or 6 months, respectively. In conclusion, LP induces in the GCL selective RGCs loss that does not progress after 1 month, and S- and L-cone loss that progresses for up to 6 months. Thus, OHT results in severe damage to both the innermost and the ORL.

1. Introduction

It is well recognized that in glaucomatous optic neuropathies (GONs) there is a progressive loss of retinal ganglion cells (RGCs) which results in structural alterations of the nerve fiber layer and the optic disc and in functional deficits that with time progress to blindness (Lei et al., 2008; Choi et al., 2011; Savini et al., 2011, 2013).

To better understand the mechanisms causing RGC degeneration in GONs, the effects of a variety of insults possibly implicated in this pathology have been investigated, including; i) optic nerve lesion induced by complete intraorbital optic nerve transection (Vidal-Sanz et al., 2002; Alarcón-Martínez et al., 2009, 2010) (IONT) or crush (Parrilla-Reverter et al., 2009); ii) transient ischemia of the retina induced by elevation of the intraocular pressure above systolic levels (Sellés-Navarro et al., 1996) or by selective ligature of the ophthalmic vessels (Lafuente López-Herrera et al., 2002; Avilés-Trigueros et al., 2003; Mayor-Torreglosa et al., 2005; Vidal-Sanz et al., 2007) or; iii) ocular hypertension (OHT) (Morrison et al., 2005, 2011) achieved by a variety of methods including episcleral vein cauthery (Garcia-Valenzuela et al., 1995), hypertonic saline injection of the humor outflow pathways (Morrison et al., 1997), limbar laser photocoagulation (Quigley and Hohman, 1983; WoldeMussie et al., 2001; Vidal-Sanz et al., 2012) or injection of microspheres into the anterior chamber (Sappington et al., 2010).

* Corresponding author. Dpto Oftalmología, Facultad de Medicina, Universidad de Murcia, IMIB-Arrixaca, Campus de Espinardo, 30100, Spain.
E-mail address: manuel.vidal@um.es (M. Vidal-Sanz).
[1] Joint first authors.

http://dx.doi.org/10.1016/j.exer.2015.01.006

Because elevated intraocular pressure (IOP) remains the main treatable risk factor in GON (The AGIS investigators, 2000; Morrison et al., 2008), a large variety of animal models have implemented OHT as the main feature to study the effects of elevated IOP on the primary visual pathway. This approach has provided advances in our understanding of OHT-induced RGC, optic nerve and retinofugal projection's pathology (Filippopoulos et al., 2006; Schlamp et al., 2006; Howell et al., 2007; Morrison et al., 2008; Soto et al., 2008; Almasieh et al., 2012; Calkins, 2012; Vidal-Sanz et al., 2012).

Whether glaucoma induces loss of retinal neurons other than the RGCs has remained controversial (Panda and Jonas, 1992; Kendell et al., 1995; Wygnanski et al., 1995; Kielczewski et al., 2005). However, several morphological (Lei et al., 2008; Kanis et al., 2010; Choi et al., 2011; Werner et al., 2011) and functional studies (Holopigian et al., 1990; Drasdo et al., 2001; Velten et al., 2001; Werner et al., 2011) support the idea that in addition to RGC loss there are losses of other neurons in the outer nuclear layer of GON human retinas. In OHT murine models of GON, other non-RGC neurons were also found affected in various studies using electroretinogram (ERG) recordings and measuring retinal layer thickness (Korth et al., 1994; Mittag et al., 2000; Bayer et al., 2001; Holcombe et al., 2008; Kong et al., 2009; Salinas-Navarro et al., 2009a; Cuenca et al., 2010; Georgiou et al., 2014). Moreover, several recent studies in rodent models of LP-induced OHT have shown an activation of macro and microglia not only in the retina of the OHT eye but also in the fellow normotensive eye (Ramírez et al., 2010; Gallego et al., 2012; de Hoz et al., 2013) and such a microglia activation was not only present in the ganglion cell layer but also in the inner and outer retinal layers (Rojas et al., 2014).

However, to the best of our knowledge there have been no investigations examining the entire populations of cells in the ganglion cell layer (GCL), nor the population of cone photoreceptors in murine models of OHT short or long periods of time after laser photocoagulation (LP). The present studies are conducted on a rat model of OHT based on the LP of the limbar and perilimbar tissues of the eye (WoldeMussie et al., 2001; Levkovitch-Verbin et al., 2002; Salinas-Navarro et al., 2009a, 2009b, 2010; Cuenca et al., 2010; Nguyen et al., 2011; Vidal-Sanz et al., 2012), and use retrogradely transported neuronal tracers, nuclear staining and molecular markers to identify RGCs, cells in the GCL and L- and S-cone outer segments. In addition we have quantified by western blotting the expression of the three opsins and measured retinal thickness in cross-sections. Finally, we have used our recently developed technology to count the total population of these cells and image their topological distribution within the retina (Schnebelen et al., 2009; Salinas-Navarro et al., 2009a, 2009b, 2010; Nadal-Nicolás et al., 2009, 2012; Ortín-Martínez et al., 2010, 2014; Vidal-Sanz et al., 2012; Dekeyster et al., 2015). Specifically we asked whether long after LP: i) There is loss of other non-RGC neurons within the GCL; ii) Cone-photoreceptors are also affected, and; iii) The loss of cones is topologically related to RGC-loss. Short accounts of this work were reported in abstract format (Salinas-Navarro et al., 2011, ARVO E-Abstract 2459; Ortín-Martínez et al., 2012, ARVO E-Abstract 2488).

2. Material and methods

2.1. Animal handling

Experimental procedures were in accordance with the ARVO and European Union guidelines for the use of animals in research and approved by the Ethical and Animal Studies Committee of the University of Murcia. Adult female albino Sprague Dawley (SD) rats (180–230 g) (Charles River Laboratories, L'Arbresle, France) were housed at University of Murcia animal facilities. Surgeries and IOP measurements were performed under anesthesia intraperitoneal (ip) injection of xylazine (10 mg/kg body weight, Rompun; Bayer, Kiel, Germany) and ketamine (60 mg/kg bw, Imalgene; Merial Laboratorios, Barcelona, Spain). During recovery topical ointment containing Tobramycin (Tobrex®, Alcon Cusí, S.A. Barcelona, Spain) was applied to the eyes to prevent corneal desiccation. Rats were given oral analgesia (Buprex, Buprenorphine 0.3 mg/ml Schering-Plough, Madrid, Spain) at 0.5 mg/kg (prepared in strawberry-flavored gelatin) the day of surgery and during the next 10 days. Animals were sacrificed with an ip overdose of 20% sodium pentobarbital (Dolethal Vetoquinol®, Especialidades Veterinarias, S.A., Alcobendas, Madrid, Spain).

A total of 108 SD rats were used in this study. In all animals, the left eyes were used as experimental eyes whereas the fellow uninjured right eyes were used as control. Recent studies indicate that injury to one eye may produce significant molecular and structural changes in the intact contralateral eye (Bodeutsch et al., 1999; Lönngren et al., 2006; Ramírez et al., 2010; Gallego et al., 2012; de Hoz et al., 2013; Rojas et al., 2014), thus for western blotting (WB) experiments we used naïve (intact) animals as control.

2.2. Experimental design

The study addressed three main questions regarding the short- and long-term effects of LP-induced OHT in the adult rat retina: i) Does OHT affect other non-RGC neurons in the ganglion cell layer (GCL)?; ii) Does OHT affect the outer retina?, and; iii) The loss of cone-photoreceptors observed after OHT, could it be related to RGC loss? (Fig. 1). To answer these questions two main groups of animals were prepared; one in which OHT was induced by LP to study the effects of this intervention in the inner and outer retina, and; a second one in which the optic nerve was intraorbitally divided to provoke axotomy-induced RGC degeneration and thus to observe whether this massive loss of RGCs was followed by photoreceptor degeneration. In addition, to demonstrate that the observed retinal degeneration is not light-mediated a sham operated control group was analyzed one month after lasering the non-draining portion of the sclera.

2.3. Animal manipulations

OHT was achieved by LP (Viridis Ophthalmic Photocoagulator-532 nm laser; Quantel Medical, Clermont-Ferrand, France) of the trabecular meshwork, the perilimbar and episcleral vessels following methods (WoldeMussie et al., 2001; Levkovitch-Verbin et al., 2002) previously described in detail that are standard in our Laboratory (Salinas-Navarro et al., 2009a, 2009b, 2010; Cuenca et al., 2010; Vidal-Sanz et al., 2012). In the Sham group of rats, the laser beam was aimed at the non-draining portion of the sclera, specifically 1.2 mm posterior to the limbus of the left eyes to avoid the aqueous collection system, as described previously (de Hoz et al., 2013). In both the Sham and experimental groups the spot size, duration and power used were 50–100 μm, 0.5 s and 0.4 W, respectively. In both the experimental and sham groups, the left eyes received between 85 and 90 laser burns (Salinas-Navarro et al., 2010; Vidal-Sanz et al., 2012). IOP was monitored bilaterally prior to, and at 12, 24, 48 h, 3 days, 1 or 2 weeks, 1, 3 or 6 months after LP with a rebound tonometer (Tono-Lab; Tiolat, OY, Helsinki, Finland) (Salinas-Navarro et al., 2009a, 2009b, 2010). With the exception of the readings taken at 12 h after LP, all other measurements were obtained at the same time in the morning to avoid IOP fluctuations due to circadian rhythms (Krishna et al., 1995; Moore et al., 1996; Jia et al., 2000), or to elevation of the IOP itself (Drouyer et al., 2008).

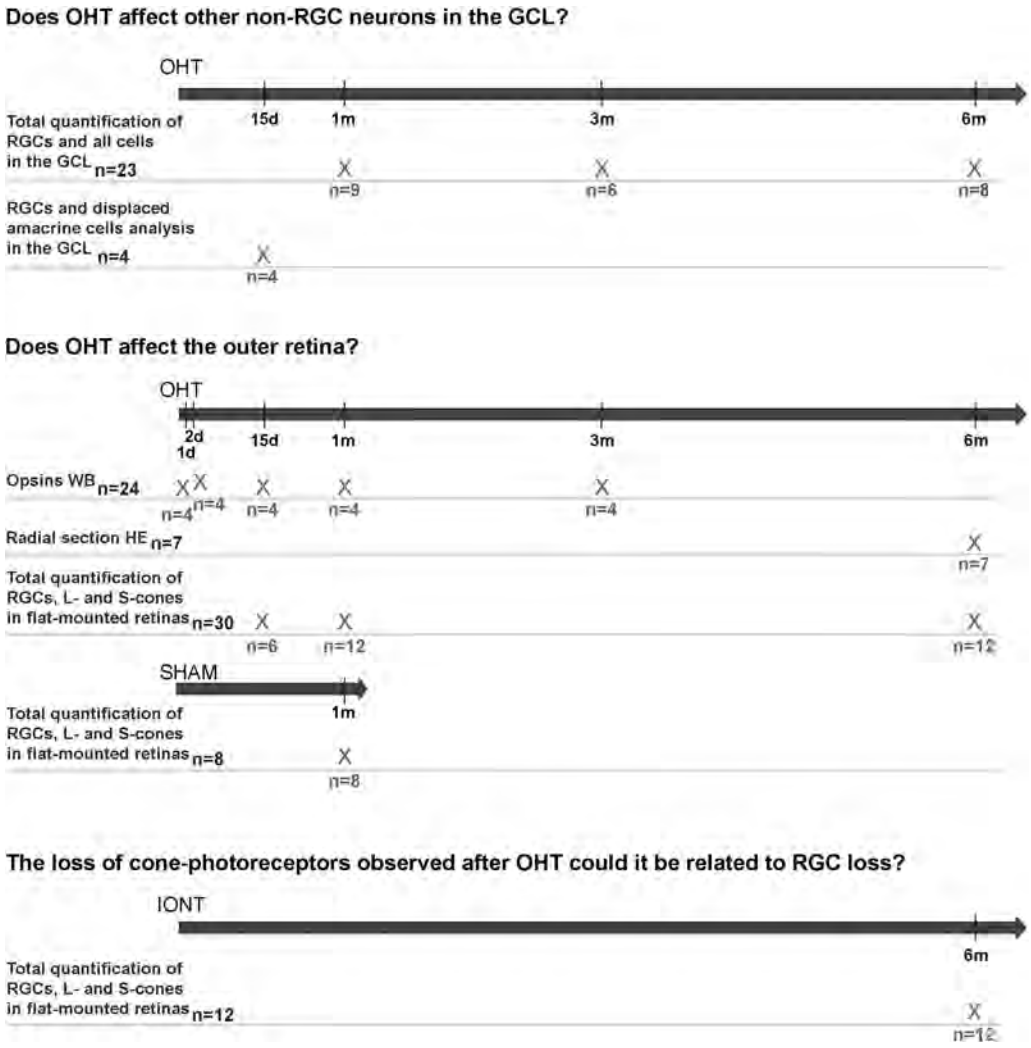

Fig. 1. Experimental design. Outline of the time frame, animals and techniques employed to address the following questions 1. Does OHT affect other cells in the GCL besides RGCs? For this: i) the total number of $Brn3a^{+}$RGCs and $DAPI^{+}$nuclei in the GCL layer was quantified in retinal whole-mounts and their distribution illustrated with isodensity maps, and; ii) the population of RGCs was traced with FG and immunodetected with Brn3a and displaced amacrine cells were immunodetected with Calretinin antibodies. 2. Does OHT have an effect on the outer retinal layers? to respond this question we have: i) measured the expression level of the three opsin proteins by western blotting (WB) in extracts from naïve retinas and retinas dissected after LP; ii) measured the thickness of the retina and outer nuclear layer in radial cross-sections stained with hematoxylin/eosin (HE) at 6 months after LP; iii) quantified the total number of L- and S-cones and evaluated their topological distribution after LP in retinal whole-mounts doubly immunodetected with both cone-opsins and: iv) quantified the number of RGCs, L-cones and S-cones in SHAM controls, to demonstrate that lasering the non-draining portion of the sclera does not have an effect on the RGC, L- or S-cone populations, and rule out that the observed retinal degeneration is light-mediated. 3. Could the loss of cone photoreceptors after OHT be related to RGC loss? To answer this question the total number and topography of RGCs, S- and L-cones in two different experimental situations leading to massive RGC death were compared: i) Fifteen days, one and six months after LP-induced OHT (see 2. iii), and; ii) Six months after intraorbital optic nerve transection.

The left optic nerve was intraorbitally transected at approximately 0.5 mm from the optic disc (Villegas-Pérez et al., 1993; Avilés-Trigueros et al., 2000; Vidal-Sanz et al., 2002; Alarcón-Martínez et al., 2009).

RGCs were identified with Fluorogold® (FG; Fluorochrome Corp, Denver, CO, USA) (3% diluted in 10% DMSO-saline) applied to both superior colliculi (SCi) one week before animal processing as reported (Vidal-Sanz et al., 2000; Salinas-Navarro et al., 2009a, 2009b), or with Brn3a immunohistochemistry (Nadal-Nicolás et al., 2009, 2012, 2014).

2.4. Tissue processing

After deep anesthesia rats were sacrificed and perfused transcardially with 4% paraformaldehyde (PFA) in 0.1 M phosphate buffer (PB) after a saline rinse.

2.5. Western blot analysis

Left retinas from naïve and experimental animals (see Fig. 1 for details) were fresh dissected and protein extracted and subjected to standard electrophoresis (Agudo et al., 2008, 2009). Membranes were incubated with different opsin antibodies (for details see Table 1), using β-actin as loading control. HRP-conjugated secondary antibodies were visualized by chemiluminescence (ECL, Amersham Pharmacia Biotech), the signal was acquired with TyphoonTM 9410 (Global Medical Instrumentation, Inc., Ramsey, MN, USA) and analyzed with ImageJ (Rasband, 1997–2014) gel analysis tool.

2.6. Flat mounted retinas, DAPI staining and immunohistofluorescence

To study cone photoreceptors, the L- and S-cones were double immunodetected by their specific opsin expression (Ortín-

Table 1
Primary and Secondary antibodies employed.

Antigen	Primary antibody	Western blotting	IHF	Source
Rhodopsin (Rods)	Mouse anti-opsin	1:500	#	Sigma–Aldrich (Alcobendas, Madrid, Spain)
Human red/green opsin (L-cones)	Rabbit anti-opsin red/green	1:500	1:1200	Chemicon-Millipore Iberica (Madrid, Spain)
Blue opsin (S-cones)	Goat anti-OPN1SW (N20)	1:500	1:1000	Santa Cruz Biotechnologies (Heidelberg, Germany)
β-actin	Rabbit anti-β-actin	1:500	#	Sigma–Aldrich (Alcobendas, Madrid, Spain)
Brn3a (RGCs)	Goat anti-Brn3a (C-20)	#	1:750	Santa Cruz Biotechnologies (Heidelberg, Germany)
Iba1 (Microglial cells)	Rabbit anti-Iba1	#	1:1000	Wako Chemical GmbH (Neuss, Germany)
Calretinin (RGCs and Amacrine cells)	Rabbit anti-calretinin	#	1:2500	Swant (Marly, Switzerland)

Secondary antibody	Western blotting	IHF	Source
Donkey anti-mouse HRP IgG (H + L)	1:7500	#	Santa Cruz Biotechnologies (Heidelberg, Germany)
Donkey anti-rabbit HRP IgG (H + L)	1:7500	#	Santa Cruz Biotechnologies (Heidelberg, Germany)
Donkey anti-goat HRP IgG (H + L)	1:15,000	#	Santa Cruz Biotechnologies (Heidelberg, Germany)
Donkey anti-rabbit Alexa 594 IgG (H + L)	#	1:500	Molecular Probes (Life Technologies, Madrid, Spain)
Donkey anti-goat Alexa 488 IgG (H + L)	#	1:500	Molecular Probes (Life Technologies, Madrid, Spain)
Donkey anti-goat Alexa 594 IgG (H + L)	#	1:500	Molecular Probes (Life Technologies, Madrid, Spain)
Donkey anti-rabbit Alexa 488 IgG (H + L)	#	1:500	Molecular Probes (Life Technologies, Madrid, Spain)

IHF: Immunohistofluorescence.

Martínez et al., 2010, 2014; García-Ayuso et al., 2013). In these same retinas, RGCs were identified by FG tracing in the OHT groups, and by Brn3a immunodetection in the groups used to study the GCL as well as in the IONT group (Nadal-Nicolás et al., 2012). The GCL of the rat contains RGCs, vascular endothelial cells, microglia and a population of displaced amacrine cells as numerous as the population of RGCs itself (Perry and Cowey, 1979; Perry, 1981; Schlamp et al., 2013). Thus, to study cells in this layer, retinal wholemounts were stained with DAPI (Vectashield mounting medium with DAPI 1.5 μg/ml; Vector Laboratories, Inc., Burlingame, CA, USA) to identify all the cell nuclei in the GC layer and immunostained with antibodies against Brn3a, Calretinin and Iba1 to identify RGCs (Nadal-Nicolás et al., 2014), amacrine cells (Dijk and Kamphuis, 2004) and microglia (Rojas et al., 2014), respectively (Table 1).

2.7. Image analysis

Retinas were examined and photographed with a microscope (Axioscop 2 Plus; Zeiss) equipped with a digital-high-resolution camera (ProgRes™ c10; Jenoptic, Jena, Germany) and a computer-driven motorized stage (ProScan™ H128; Prior Scientific Instruments Ltd., Cambridge, UK) connected with an image analysis system (Image-Pro Plus 5.1 for Windows®; Media Cybernetics, Silver Spring, MD) and a microscope controller module (Scope-Pro 5.0 for Windows®; Media Cybernetics). Flat mounted retinas or retinal cross-sections photomontages were constructed from 144 consecutive frames captured on the microscope side by side with no gap or overlap between them.

2.8. Automated study of retinal cell populations, layer thickness and isodensity maps

FG^+RGCs, $Brn3a^+$RGCs, $DAPI^+$nuclei, Immunolabelled L- and S-cones were quantified automatically and the data were translated into isodensity maps to allow the visualization of cell distribution, as reported (Salinas-Navarro et al., 2009a, 2009b, 2010; Nadal-Nicolás et al., 2009, 2012; Ortín-Martínez et al., 2010, 2014; Vidal-Sanz et al., 2012). Isodensity maps are color-coded representations of filled contour plots created with the graphic software Sigmaplot® 9.0 (Systat Software Inc., Richmond, CA). Whole-mount reconstructions were prepared with the aid of a motorized stage on a photomicroscope with a high-resolution camera connected to an image analysis system (Image-Pro Plus 5.1; Media Cybernetics, Silver Spring, MD, USA). Retinal multiframe acquisitions were photographed in a raster scan pattern where the frames were captured contiguously side-by-side with no gap or overlap between them. Isodensity maps demonstrating the topological distribution of FG^+RGCs, $Brn3a^+$RGCs, $DAPI^+$nuclei, Immunolabelled L- and S-cones are filled contour plot generated by assigning to each one of the appropriate subdivisions of each individual frame a color code according to its density value within a 28-step color scale. $Iba1^+$cells were counted manually in standard areas of the retinas and the results extrapolated as reported (Sobrado-Calvo et al., 2007) and $Calretinin^+$cells were examined and photographed under the fluorescence microscope.

For cross-section analysis, eyes were embedded in paraffin (García-Ayuso et al., 2010). Three-micron-thick cross-sections cut in the parasagittal plane comprising the superior and the inferior retina within the width of the optic nerve (ON) head, were obtained in a microtome (Microm HM-340-E; Microm Laborgerate GmbH, Walldorf, Germany) and subjected to hematoxylin-eosin staining (García-Ayuso et al., 2010). From each retina three radial sections were analyzed. Note that in this analysis, only the narrow band of the mid-sagittal plane of the retina was studied, sparing the nasal and temporal side of the retina. Retinal layer thickness was measured in the photomontages with a semi-automated routine developed with Image-Pro Plus 5.1 macro language. Twenty sampling areas with a fixed radius of 0.16 mm were distributed along the radial section, 10 in the superior and 10 in the inferior retina. The limit of the retinal layer of interest was traced and the average distance between lines was measured automatically. Data from each animal was averaged and pooled for each experimental or control group.

2.9. Statistical analysis

All data are shown as the mean ± SD, and differences considered significant when $p < 0.05$. Statistical analysis was done using Sigmastat® 3.1 for Windows® (SigmaStat® for Windows™, version 3.11; Systat Software, Inc., Richmond CA, USA). Kruskal Wallis test was used when comparing more than two groups and T-test or Mann–Whitney test when comparing two groups only. Correlation analysis were done between the cumulative IOP elevations, calculated as described by Levkovitch-Verbin et al. (2002), or the IOP peaks observed during the first two weeks and the degree of RGC, L- and S-cone loss for each retina and animal of the groups analyzed at 15 days ($n = 6$), 1 ($n = 10$) and 6 months ($n = 10$) after LP-induced OHT.

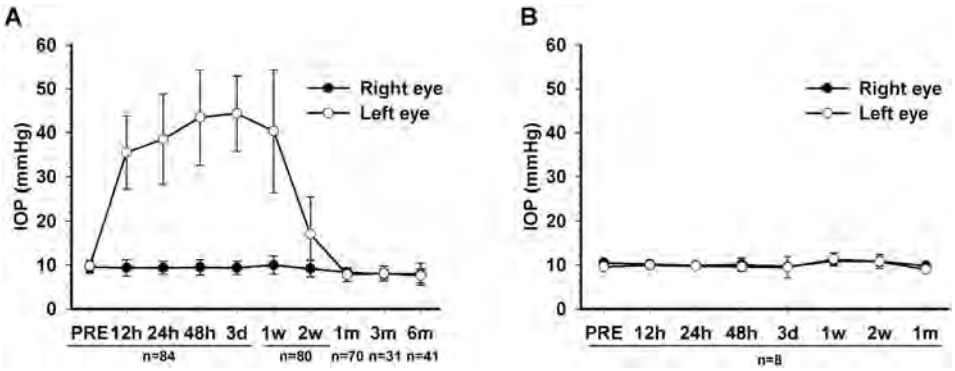

Fig. 2. Intraocular pressure (IOP) readings. A, B. Histograms representing the mean (±SD) IOP measured at each time point after LP-induced OHT (A) and after LP of the non-draining portion of the sclera (B) and those registered prior to lasering (PRE) in the right (black circles) and left eyes (open circles). At each time point 8 consecutive IOP readings were carried out for each eye and averaged. T-test analysis $p < 0.05$ from 12 h to 2w for values shown in A.

3. Results

3.1. Laser photocoagulation induces OHT

Following LP, IOP raises significantly during the first 24 h reaching maximal values at approximately 48 h. These values were maintained for the first week and then decline slowly to reach basal values by one month, in agreement with previous reports (Salinas-Navarro et al., 2010) (Fig. 2A).

3.2. OHT does not affect non-RGC neurons in the GCL

To investigate the fate of neurons in the retinal ganglion cell layer (GCL), the total numbers of Brn3a$^+$RGCs and DAPI$^+$nuclei were counted automatically, and their distribution visualized with isodensity maps for each experimental and contralateral retinal-wholemount analyzed from 1 to 6 months following LP. The right retinas showed a normal distribution of Brn3a$^+$RGCs with higher densities in a region along the nasotemporal axis on the superior retina while the LP-left retinas showed typical regions lacking Brn3a$^+$RGCs within pie-shaped sectors (Figs. 3 and 4). The mean total numbers of Brn3a$^+$RGCs (±SD) in the right and left retinas analyzed 1 (n = 9), 3 (n = 6) or 6 (n = 8) months after LP were 86,717 ± 5318 and 19,342 ± 9,007, 85,695 ± 10,858 and 13,084 ± 7809 or 83,878 ± 4467 and 35,889 ± 23,845, respectively (Fig. 5). The total numbers of Brn3a$^+$RGCs in the right eyes of the retinas examined 1, 3 or 6 months were comparable (Kruskal–Wallis test, p = 0.453), but significantly greater than their contralateral LP retinas at each time point examined (T-test, $p \leq 0.001$ for 1, 3 or 6 months respectively).

When examined for DAPI$^+$nuclei, the GCL of the right retinas showed a distribution of nuclei throughout the retina that paralleled, but greatly outnumbered, the distribution of Brn3a$^+$RGCs (Fig 3). Total numbers DAPI$^+$nuclei in the right eyes of the retinas

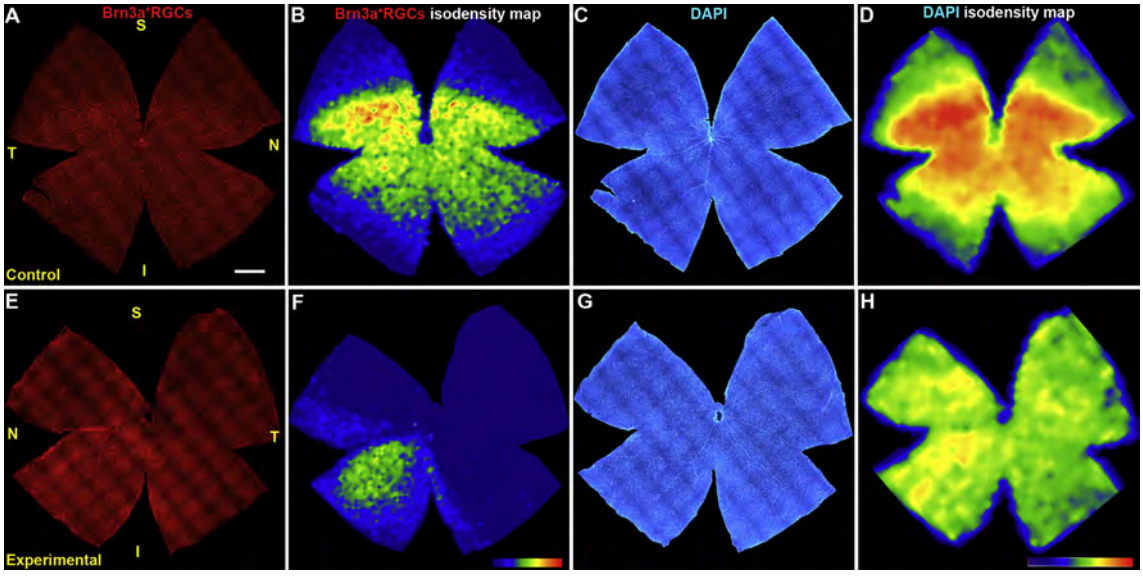

Fig. 3. Topological distribution of Brn3a$^+$RGCs and DAPI$^+$nuclei 3 months after LP. A–D. Wholemount of a representative control right retina immunoreacted for Brn3a (A) and stained with DAPI (C), and their corresponding isodensity maps (B, D). E–H. Wholemount of a representative experimental left retina 3 months after laser photocoagulation (LP) of the perilimbar and limbar tissues immunoreacted for Brn3a (E) and its isodensity map (F) which shows absence of Brn3a$^+$RGCs in a large sector that extends approximately from 10 to 5 o'clock orientation. Such a lack of Brn3a$^+$RGCs is clearly observed in the isodensity map (F) where such a sector acquires a dark blue color implying lack of Brn3a$^+$RGCs. The same retina shows large numbers of DAPI$^+$nuclei in the areas lacking Brn3a$^+$RGCs (G) as shown in its isodensity map (H), suggesting that LP does not affect other non-RGCs in the GCL. Density color scale ranges from 0 (dark blue) to 3500 or higher (red) Brn3a$^+$RGCs/mm^2, or from 0 (purple) to 6000 or higher DAPI$^+$nuclei/mm^2 (red). For all retinas the dorsal pole is orientated at the 12 o'clock position. Scale bar = 1 mm.

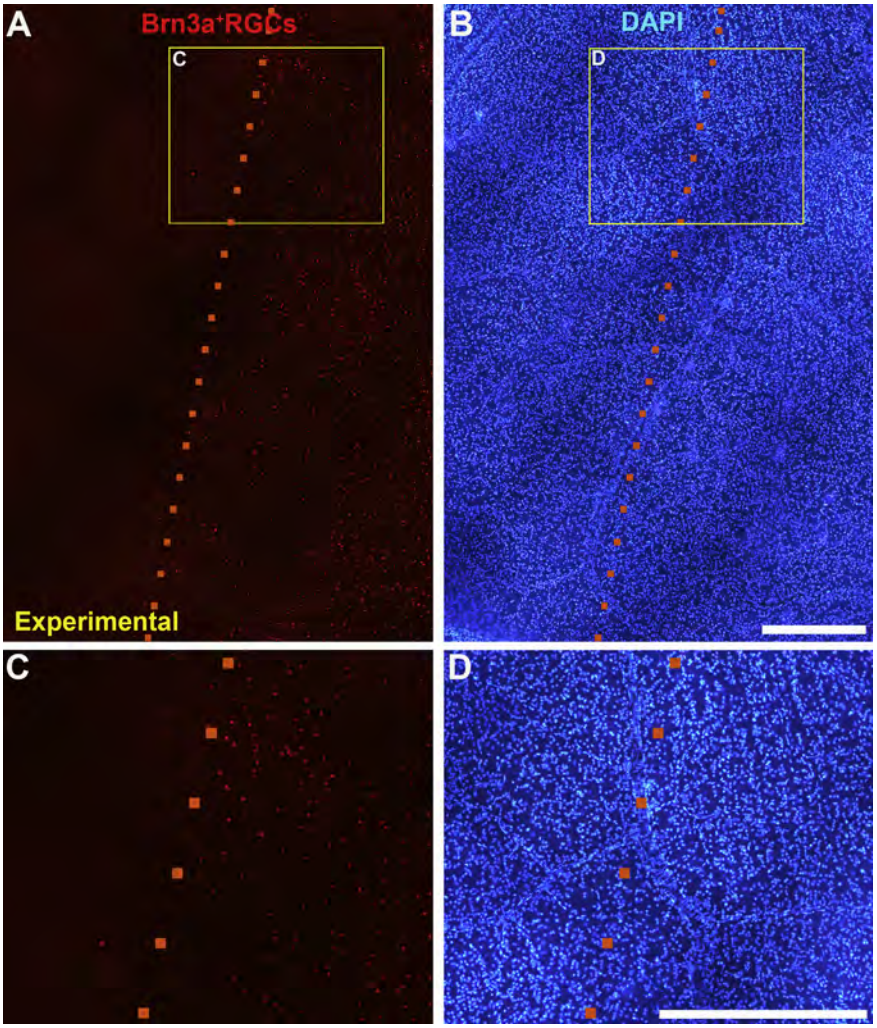

Fig. 4. OHT induces loss of RGCs but not other cells in the GCL. A–B. Micrographs from a representative experimental retina analyzed 3 months after LP and stained for Brn3a (A) and DAPI (B), showing in the border (dashed line) of a typical sector devoid of Brn3a$^+$RGCs (A). Within the sector lacking Brn3a$^+$RGCs, there are large numbers of DAPI stained nuclei in the GCL (B). C–D are inserts from A and B, respectively. Scale bars for A–B = 500 μm. C–D = 200 μm.

examined 1, 3 or 6 months were comparable (Kruskal–Wallis test, $p = 0.13$). This was in contrast with the absence of areas lacking Brn3a$^+$nuclei in the LP-retinas, furthermore within the areas lacking Brn3a$^+$RGCs there were large numbers of DAPI$^+$nuclei (Figs. 3 and 4). The mean total numbers of DAPI$^+$nuclei (±SD) for the left retinas represented 82, 78 or 71% of their fellow retinas 1, 3 or 6 months after LP (Fig 5), and these data were significantly smaller when compared to their right fellow retinas (T-test, $p \leq 0.001$ for 1, 3 or 6 months respectively). The areas devoid of Brn3a$^+$RGCs presented however large numbers of DAPI$^+$nuclei, many of which are presumably displaced amacrine cells and a small proportion are microglial cells (Fig. 6). In the retinas examined 15 days after LP ($n = 4$) and one week after FG application to their SCi, within the areas devoid of FG$^+$RGCSs and Brn3a$^+$RGCs there were large numbers of Calretinin$^+$cells, indicating that some of the cells present in these sectors were indeed displaced amacrine cells (Fig. 6). Iba1$^+$cells were counted manually in a few LP-retinas and their total estimates were 29,529, 21,668 or 5482 at 1($n = 3$), 3($n = 3$) or 6 ($n = 3$) months respectively, and represent 17, 12 or 3% of the total number of DAPI$^+$nuclei, respectively. There were statistically significant differences between the numbers of Iba1$^+$cells at 6 months when compared to those obtained at 1 or 3 months (Mann–Whitney test, $p \leq 0.01$).

3.3. OHT results in downregulation of the expression of rod- and cone-opsins

WB analysis shows downregulation of rhodopsin, L- and S-opsin. By two weeks after LP the levels of rhodopsin and L-opsin had diminished significantly to nearly 60%, from 15 days to 1 month there were further significant reductions for all opsins and by 3 months approximately 20% of the original protein levels were quantified (Fig. 7).

3.4. Cross-section analysis shows areas of focal degeneration

Control retinas showed typical layered appearance (Fig. 8). The left OHT-retinas at 6 months showed predominantly areas with normal appearance (Fig. 8A) but also presented multiple small focal areas of degeneration whose location, number and severity varied within different animals (Fig 8 B–H). These focal areas showed what appeared to be different stages of outer nuclear layer and outer external segments layer (ONL and OSL) degeneration (Fig. 8C–H). Morphometric analysis of the thickness of the ONL and of all retinal layers shows on average significant reductions for the LP-retinas (Fig. 8I), that amounted to 30% and 17%, for the ONL (T-test

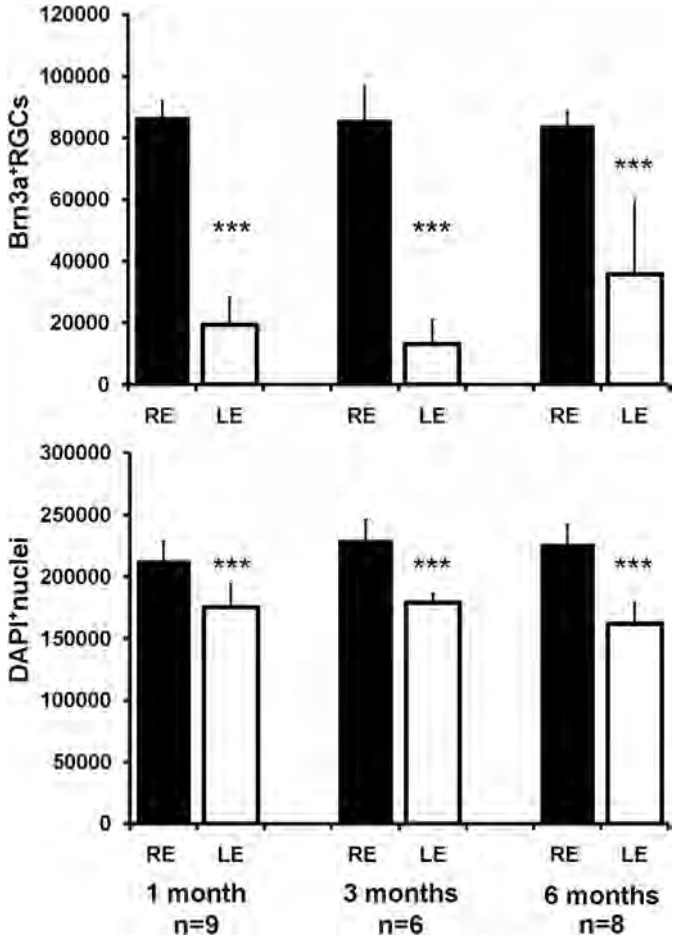

Fig. 5. Total numbers of Brn3a$^+$RGCs or DAPI$^+$nuclei 1, 3 or 6 months after lasering. Histograms representing mean (±SD) total numbers of Brn3a$^+$RGCs (Top) or DAPI$^+$nuclei (Bottom) in the same right (RE) or left (LE) retinas 1–6 months after lasering the LE. The total numbers of Brn3a$^+$RGCs or DAPI$^+$nuclei in the right retinas were comparable (Kruskal–Wallis test, $p = 0.453$ or $p = 0.13$ for Brn3a + RGCs or DAPI + nuclei, respectively). The total numbers of Brn3a$^+$RGCs in the left eyes represented 22, 15 and 43% of the total numbers of Brn3a$^+$RGCs found in their fellow retinas at 1, 3 or 6 months (T-test, $p \leq 0.001$ (***), for all groups), while the total numbers of DAPI$^+$nuclei in the left eyes represented, at the same time points 82, 78 and 71% of the original DAPI$^+$nuclei population, T-test, $p \leq 0.001$ (***) for all groups.

$p = 0.002$) and all retinal layers (T-test $p = 0.018$) respectively (Fig. 8J, K).

3.5. Protracted loss of L- and S-cones in LP-retinas appears to be independent of RGC loss

To investigate the effect of OHT in the cone population and its correlation with RGC loss, the number and topography of L-, S-cones and RGCs were analyzed in retinas at 15 days, 1 and 6 months after LP. Table 2 shows quantitative data. The loss of RGCs was comparable to previous reports from this laboratory (Salinas-Navarro et al., 2010) and did not progress significantly from 15 days to 6 months (Fig. 9) (Table 2). With respect to cones, at 15 days total numbers of L-cones in LP eyes were comparable to their fellow eyes (T-test, $p = 0.13$) but the S-cones had lost 11% of the S-cone population in their fellow eyes (T-test, $p = 0.025$), by 1 month there was a significant decrease with losses of 19% and 33% of the original L- and S- cone population, respectively (Table 2). Between 1 and 6 months there were further significant decreases of both cone types and the losses amounted to 66% and 59% for L and S- cones, respectively (Table 2, Fig. 9). Overall in the OHT group the RGC population diminishes by 15 days and its loss does not progress further with time, whereas the populations of L- and S-cones are significantly smaller at 1 month but further diminish by 6 months.

A detailed analysis of the wholemounts together with the construction of isodensity maps (Figs. 9–11) showed a diffuse lack of cone outer segments as well as the presence of patchy areas of the retinas lacking both types of cone immunoreactive outer segments. These patchy areas (Fig. 11) may well correspond to the focal regions of outer nuclear layer degeneration observed in the radially oriented paraffin embedded cross sections of the retina that included the ON head (see section above 3.4). In the latter, within the focal region there were no cell nuclei in the ONL, indicating that in addition to L- and S-cones rods had also degenerated.

Isodensity maps show the spatial distribution of RGCs, L- and S-cones in representative control and experimental OHT retinas, and document that the topology of surviving RGCs does not match that of the surviving cones (Fig. 9). Fifteen days, 1 and 6 months after LP, retinas showed triangular sectors with their apex in the optic disc with a complete absence or a pronounced decrease in the numbers of FG$^+$RGCs. These areas lacking FG$^+$RGCs varied in size from a small sector to one or several retinal quadrants (Fig. 9). These same retinas also showed at 1 month patchy areas devoid of L- and S-opsin immunolabeling throughout the retina with an irregular distribution not related with the sectorial loss of RGCs (Figs. 9–11). These areas became bigger, more frequent and larger at 6 months (Figs. 9–11).

To investigate whether the OHT-induced cone loss was dependent on RGC loss, the cone photoreceptors were analyzed as well in retinas processed 6 months after IONT, an injury that specifically affects RGCs (Villegas-Pérez et al., 1988, 1993; Sánchez-Migallón et al., 2011). In these retinas, even though only approximately 0.1% of RGCs survived (Table 2) the populations of L-and S-cones appeared normal both in total numbers (Table 2) and topology (Figs. 9–12). Overall, in the IONT group, the RGC population is almost absent by 6 months, but the populations of L- or S-cones remain normal. There was a clear mismatch between the retinotopy of areas lacking RGCs and cone-photoreceptors.

3.6. The loss of RGCs, L- and S-cones is not correlated with cumulative IOP elevations or IOP peaks

To investigate if the levels of OHT bore a direct correlation with the degree of retinal degeneration, we analyzed the degree of RGC, L- or S-cone loss in every animal for which we had both retinas of the groups analyzed at 15 days ($n = 6$), 1 ($n = 10$) or 6 months ($n = 10$) after LP with the highest IOP recorded or the cumulative IOP elevations during the first two weeks, when IOP elevations reach their maximum values. There were no significant correlations between the IOP peaks or the cumulative IOP elevations and the degree of RGC, L- or S-cones for the three groups analyzed (for all the correlations, r^2 were smaller than 0.15 and p value >0.05).

3.7. Lasering the non-draining portion of the sclera does not result in RGC, S- or L-cone loss

To rule out the possibility that the observed retinal degeneration is light-mediated, a sham operated control group was analyzed one month after lasering the non-draining portion of the sclera. IOP measurements of the lasered eyes did not differ from the values obtained in their contralateral fellow retinas at all the time points examined (Fig. 2B). The total numbers of L-, S-cones and RGCs analyzed in both retinas from these 8 rats were comparable among them and also to data from the right eyes of the groups analyzed at 15 days, 1 or 6 months (Table 2). In all the retinas from this sham

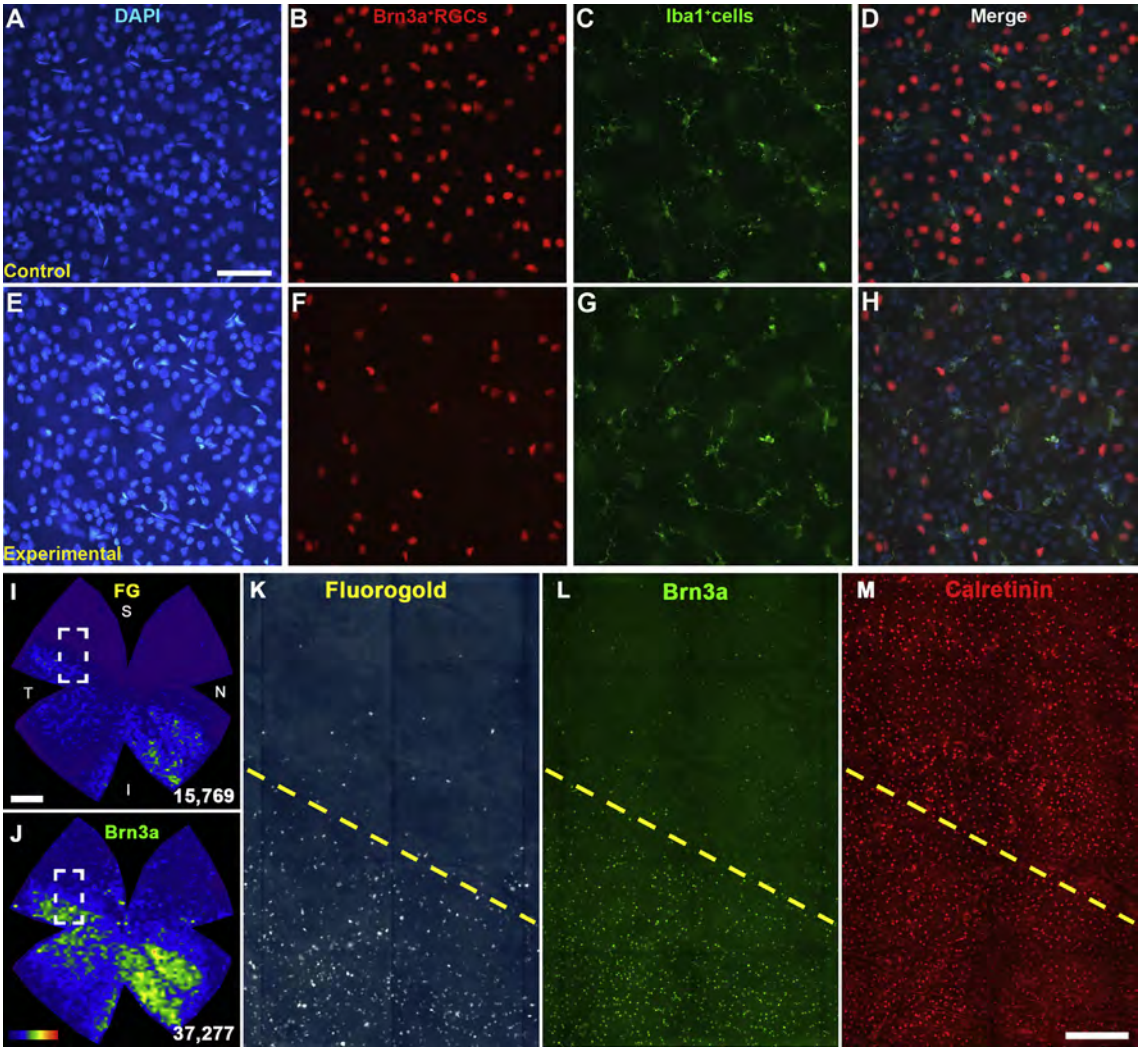

Fig. 6. The loss of RGCs is selective in the GCL. Magnifications from representative control (A–D) and experimental (E–H) retinas analyzed 3 months after LP and showing DAPI (A, E), Brn3a (B, F), Iba1(C, G) and their merged images (D, H) to illustrate that in regions lacking Brn3a$^+$RGCs there were large numbers of cell nuclei, many of which are probably displaced amacrine cells and some are Iba1$^+$ and thus microglial cells. Scale bar for A-H = 50 μm. I–J. FG and Brn3a isodensity maps showing typical pie-shaped retinal sectors lacking RGCs in an experimental retina 15 days after LP-induced OHT, retrogradely labeled with FG (I) applied to both SCi seven days prior to sacrifice to identify RGCs with an active retrograde axonal transport and immunostained with Brn3a (J) to identify surviving RGCs. As previously reported for this LP-induced OHT model, by 15 days the numbers of surviving RGCs (Brn3a$^+$RGCs) outnumber the population of FG$^+$RGCs (Salinas-Navarro et al., 2009, 2010; Vidal-Sanz et al., 2012; Nadal-Nicolás et al., 2014). Bottom right of each map: number of RGCs counted in that retina. Density color scale in J bottom left, ranges from 0 (purple) to 2500 or higher (red) RGCs/mm^2. K–M. Magnifications from the insert in I,J showing FG$^+$RGCs (K), Brn3$^+$RGCs (L) and Calretinin$^+$neurons (M) to illustrate that in the sectors of the retina lacking FG$^+$RGCs or with diminished numbers of Brn3a$^+$RGCs there were large numbers of displaced amacrine cells (Calretinin$^+$neurons) in the Ganglion Cell Layer. S: superior, I: inferior, N: nasal, T: temporal. Scale bars, I–J = 1 mm, K–M = 250 μm.

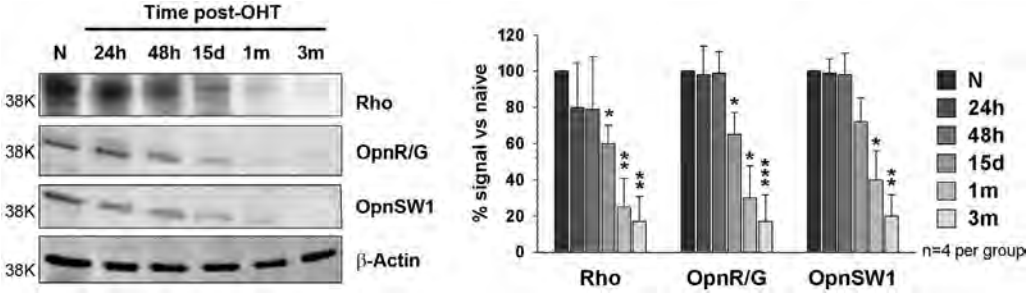

Fig. 7. Downregulation of opsin expression after OHT. Western blot time course analysis showing the regulation of rhodopsin, opsin R/G and opsin SW1 in naïve (N) and OHT-injured retinal extracts (n = 4, per group). Graph: densitometric quantification of protein signal in the experimental retinas referred to the signal in naïve extracts, which was arbitrarily considered 100%. Error bars show the SD for each experiment. β-actin was used as loading control. Statistical comparisons of each opsin values at different time points with the values obtained in naïve (N), T-test analysis: $p < 0.05$ (*); $p < 0.01$ (**); $p < 0.001$ (***).

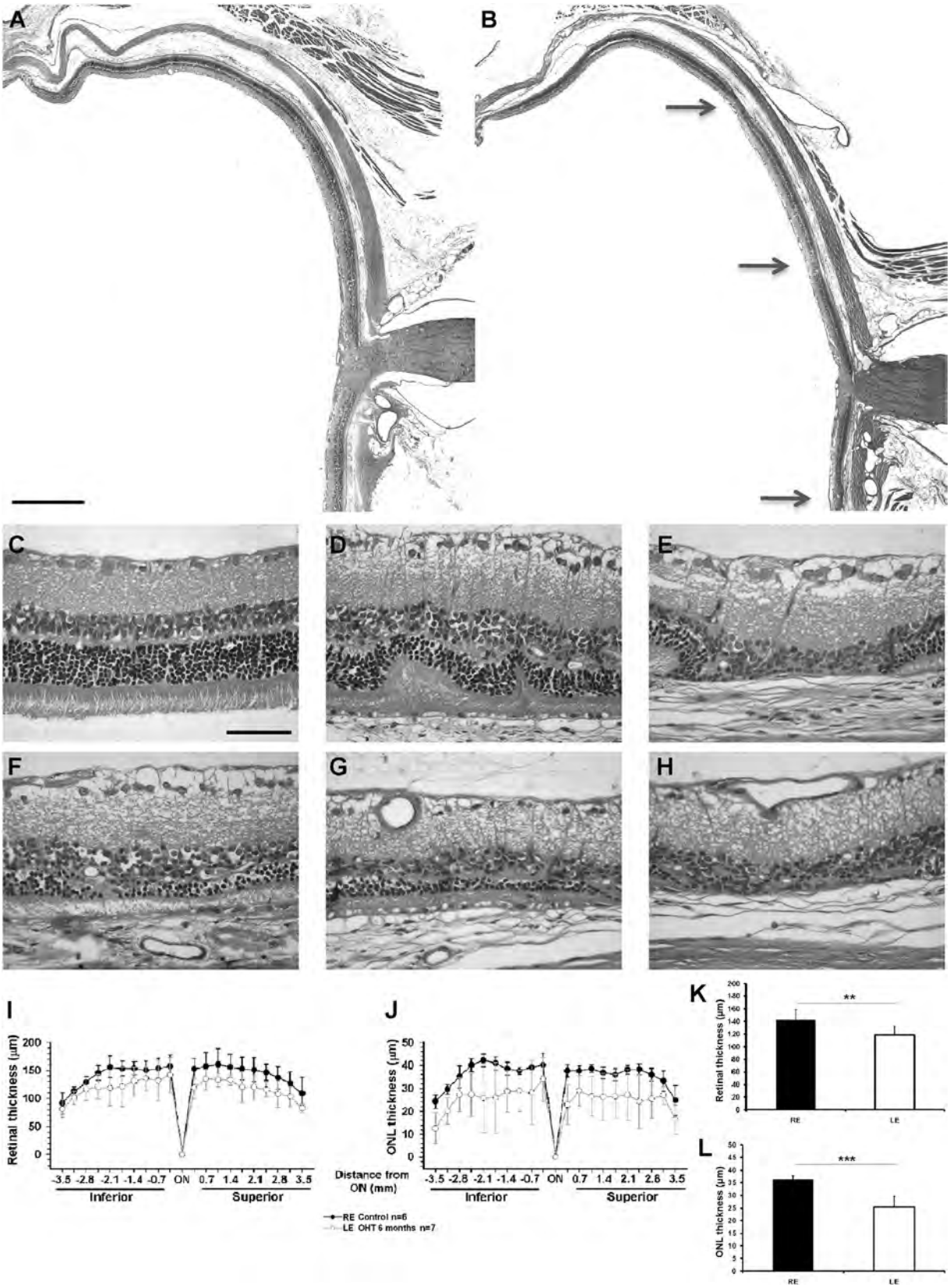

Fig. 8. Focal degeneration of outer retinal layers 6 months after OHT. A–H: Hematoxylin/eosin stained retinal cross sections 6 months after OHT showing the superior hemiretina of a control (A) and an experimental (B) retina, as well as magnifications from experimental retina showing a normal appearance (C) together with focal areas of various degrees of degeneration (D–H). Scale bar, A-B = 500 μ; C–H = 50 μm. Arrows in B indicate the presence of focal lesions. I,J: Graph showing mean (±SD) whole retinal (I) or outer nuclear layer (J) thickness in each of the 20 equidistant circular areas examined from right control (n = 6; black circles) and left experimental (n = 7; white circles) retinas 6 months after OHT. K, L: histograms showing the mean (±SD) whole retinal thickness (K) and ONL thickness (L) from control (RE) and experimental (LE) retinas. T-test analysis p = 0.018 (**); p = 0.002 (***).

Table 2
Total number of RGCs, L-cones or S-cones 1 month after Sham surgery, 15d, 1 or 6 months after OHT, or 6 months after IONT.

	SHAM 1m		OHT 15d		OHT 1m		OHT 6m		IONT 6m	
	Right retina n = 8	Left retina n = 8	Right retina n = 6	Left retina n = 6	Right retina n = 11	Left retina n = 12	Right retina n = 11	Left retina n = 11	Right retina n = 12	Left retina n = 11
RGCs	83,280# ± 3586	84,735# ± 1647	82,354*** ± 3919	24,197*** ± 22,011	78,803*** ± 4145	7706*** ± 10,672	84,065*** ± 3368	14,909*** ± 15,603	80,919*** ± 3479	84*** ± 52
L-cones	215,858# ± 19,347	225,176# ± 21,476	228,798# ± 11,004	197,093# ± 38,321	228,127*** ± 9185	184,892*** ± 21,299	204,320*** ± 15,584	70,874*** ± 43,114	215,050# ± 15,238	210,306# ± 19,658
S-cones	36,504# ± 1510	36,770# ± 1481	36,380* ± 1777	32,221* ± 3443	36,930*** ± 6970	24,287*** ± 5911	37,306*** ± 11,227	12,809*** ± 6335	34,503# ± 9030	31,210# ± 7861

The total number of RGCs, L cones and S cones in the right retinas for all the groups was comparable for each cell population (Kruskal–Wallis test $p = 0.085$, $p = 0.073$, $p = 0.954$, respectively).
Total number of the left retinas compared to those of the right retinas: No significant differences, T-test $p > 0.05$#; significant differences, T-test $p = 0.025$*, T-test $p \leq 0.001$***.

group, the topology of these retinal neurons (RGCs, L- and S-cones) had a typical normal distribution (Fig. 13).

4. Discussion

Using modern techniques to identify, count and map the populations of RGCs, cell nuclei in the GCL, L- and S-cones, we have studied short- and long-term, qualitatively and quantitatively, functionally and morphologically, the retinal changes secondary to OHT in adult Sprague Dawley rats. Our results indicate that following LP, within the GCL there is selective loss of RGCs, and with time there is progressive functional and morphological alteration of the population of S- and L-cones which do not match geographically the loss of RGCs. Thus, our data further documents that OHT results in protracted severe degeneration of the outer retinal layers.

4.1. OHT induces selective RGC loss

Examination of the GCL showed abundant DAPI$^+$nuclei in regions lacking Brn3a$^+$RGcs. Total counts of DAPI$^+$nuclei in the LP-retinas at 1, 3 or 6 months showed diminutions that could be largely explained by the magnitude of RGC loss (approximately 60–85% of the original RGC population). Because approximately 50% of the neurons in the GCL are displaced amacrine cells (Perry, 1981; Perry and Cowey, 1979; Schlamp et al., 2013) it is likely that most of the DAPI$^+$nuclei in the regions of the LP-retinas lacking Brn3a$^+$RGcs correspond to displaced amacrine cells, as was observed in these studies for Calretinin$^+$neurons in the GCL (Fig 6), as well as to a small proportion of microglia and endothelial cells. The observation of large retinal sectors lacking Brn3a$^+$RGCs in which there were abundant DAPI$^+$nuclei argues in favor of a selective damage to RGCs in the GCL while sparing other non-RGC neurons in this layer. However, there were certain discrepancies between the total numbers of Brn3a$^+$RGCs and DAPI$^+$cell counts at the time points examined. One possible explanation for such discrepancy resides in the fact that Brn3 isoforms are down-regulated prior to cell soma loss (Weishaupt et al., 2005; Nadal-Nicolás et al., 2009; Galindo-Romero et al., 2011) and this is consistent with several studies showing down-regulation of specific gene products after OHT-induced (Pelzel et al., 2012; Schlamp et al., 2001; Soto et al., 2008; Huang et al., 2006) or axotomy-induced retinal injury (Chidlow et al., 2005; Agudo et al., 2009). In addition, one should also take into consideration that LP-induced OHT is a model with a high inter-animal variability and, as such, the group analyzed at 6 months showed an overall smaller amount of RGC loss. Moreover, following RGC loss there is an important microglial response that might include proliferation and macrophage invasion (Sobrado-Calvo et al., 2007; Rojas et al., 2014) and this could also account for the increased numbers of DAPI$^+$nuclei observed after injury.

The specificity of the selective damage to RGCs in this LP-induced OHT model is further underscored by the recent observation that the typical sectorial loss also included the small population of Dogiel's RGCs, displaced to the inner nuclear layer of the retina (see Fig. 10 of Nadal-Nicolás et al., 2014). If the OHT-induced damage were to be primarily located in the GCL, the displaced RGCs would have been spared within the sectors that are typically devoid of FG-labeled RGCs, but this was not the case (Nadal-Nicolás et al., 2014). Altogether, the geographical pattern of RGC loss, including the displaced RGCs, with the presence of many non RGC-neurons (presumably displaced amacrine cells) in the GCL is in agreement with previous observations in other OHT-rodent studies showing selective loss of RGCs (Jakobs et al., 2005; Kielczewski et al., 2005; Moon et al., 2005; Cone et al., 2010) and suggests that OHT results in injury to bundles of RGC axons somewhere in the ON head,

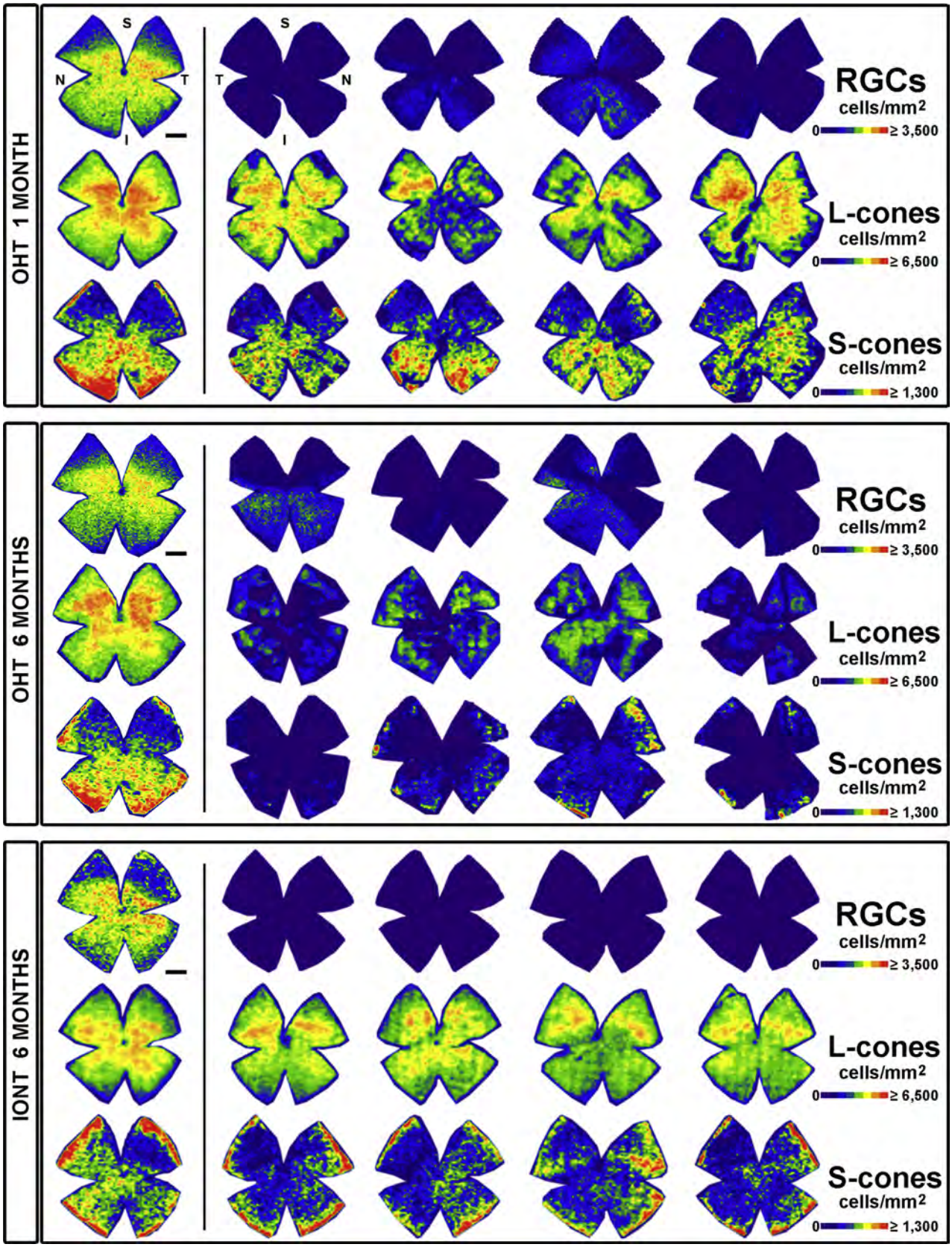

Fig. 9. Topological retinal distribution of RGCs, L-cones and S-cones after OHT or and IONT. Isodensity maps showing the distribution of surviving RGCs, L-cones and S-cones in control and experimental retinas at 1 (top panel) or 6 (middle panel) months after OHT or at 6 (bottom panel) months after IONT. For each panel the first column illustrates one representative control retina while the following correspond to four representative experimental retinas, showing the retinal distribution of the entire population of FG^{+}RGCs, L-cones or S-cones in successive rows. The RGC population was identified by FG tracing with FG applied to both superior colliculi one week prior to animal processing in groups with OHT, while in the IONT group, RGCs were immunolabeled with Brn3a. Color scale range: RGCs/mm^2 goes from 0 (purple) to 3500 or higher (red); L-cones/mm^2, from 0 (purple) to 6500 or higher (red); S cones/mm^2, from 0 (purple) to 1300 or higher (red). S: superior, T temporal, I: inferior, N: nasal. Scale bar: 1 mm.

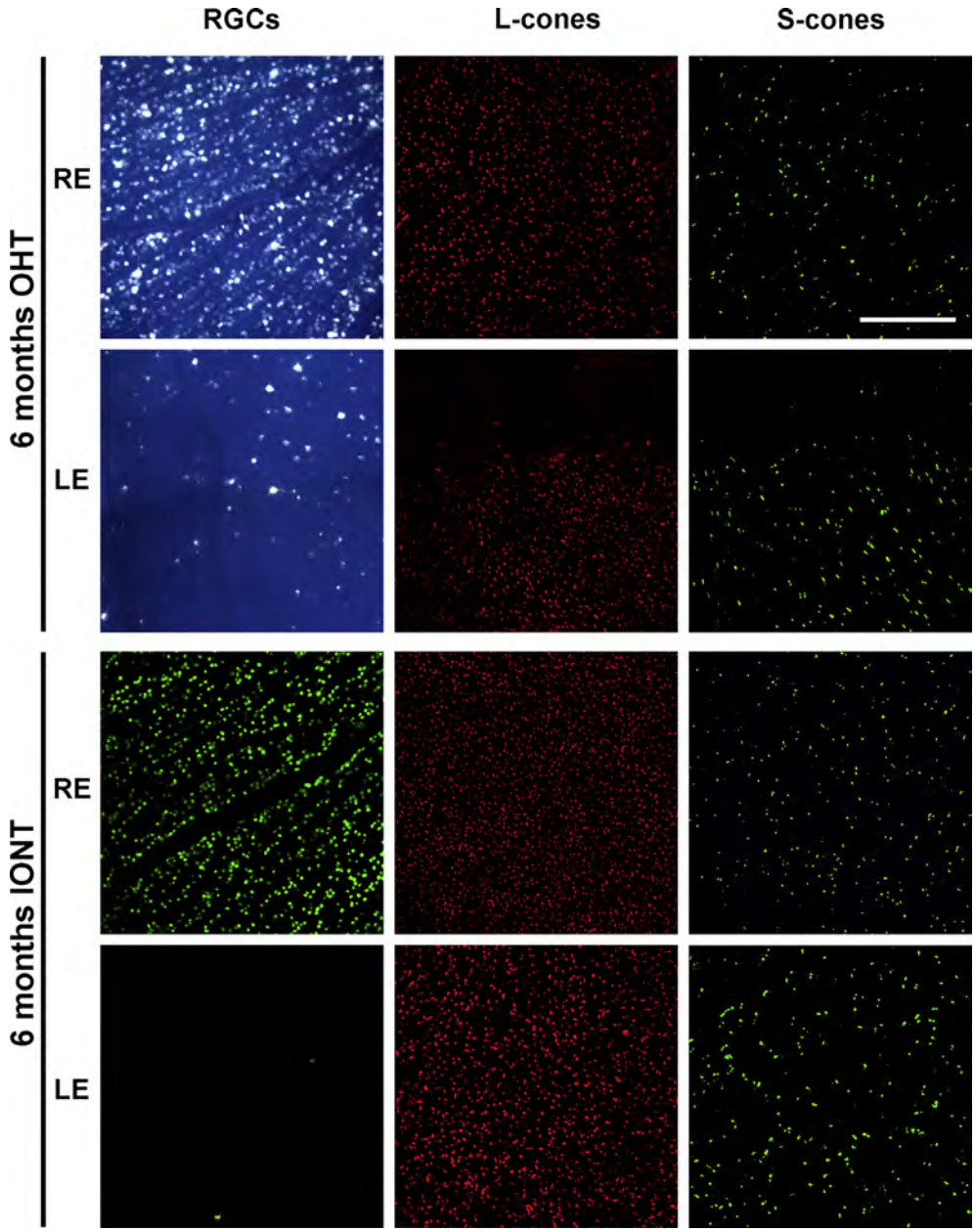

Fig. 10. LP, but not IONT, induces the loss of L and S- cones. Representative region from the inferior-temporal quadrant of control (RE) and experimental (LE) retinas 6 months alter OHT or IONT. Micrographs of the same regions show FG-traced RGCs (OHT) or Brn3a^{+}RGCs (IONT) and L- and S-cones. In the OHT experiments, the regular distribution of RGCs, L- or S-cones in the control (RE) retinas contrasts with the diminished numbers of these cells in the experimental retinas (LE). Note that in the experimental retinas RGCs are present in regions lacking cone-photoreceptors and vice versa. In the IONT experiments, the normal appearance of RGCs in the control (RE) retina contrasts with the almost complete absence of RGCs in the axotomized retina (LE), while the population of cone photoreceptors appears quite normal in both control and experimental retinas. Scale bar: 500 μm.

where axonal retinotopic arrangement is maximal (Hayreh, 1969; Quigley and Green, 1979; Quigley, 1999; Burgoyne et al., 2005; Vidal-Sanz et al., 2012), but does not result in direct damage to other non-RGC neurons present in the GCL.

4.2. OHT results in protracted degeneration of the outer retinal layer

OHT results in typical pie-shaped sectors lacking RGCs that were already evident by 15 days, as previously reported in detail (Salinas-Navarro et al., 2010, 2009b; Vidal-Sanz et al., 2012). In contrast, increased survival intervals resulted in important alterations in the outer retinal layers (ORL) with progressive diminutions in the expression of the three rat opsins, and at 6 months cross-sections revealed focal areas of severe ORL degeneration while whole-mounts showed multiple patchy areas of L- and S-cone loss. Our quantitative analysis of the cone outer-segments relies on immunodetection with corresponding opsins, thus, under-expression of these may result in diminished numbers of cones counted and mapped. In the present studies we have not quantified rods, however, cross-sections analysis in this study document that diminished expression of cone-opsins and rhodopsin correlates with an actual loss of cones and rods, rather than with a down-regulation of the opsins alone.

In monkeys with OHT induced by laser-destruction of the trabecular meshwork Pelzel et al. (2006) found no correlation

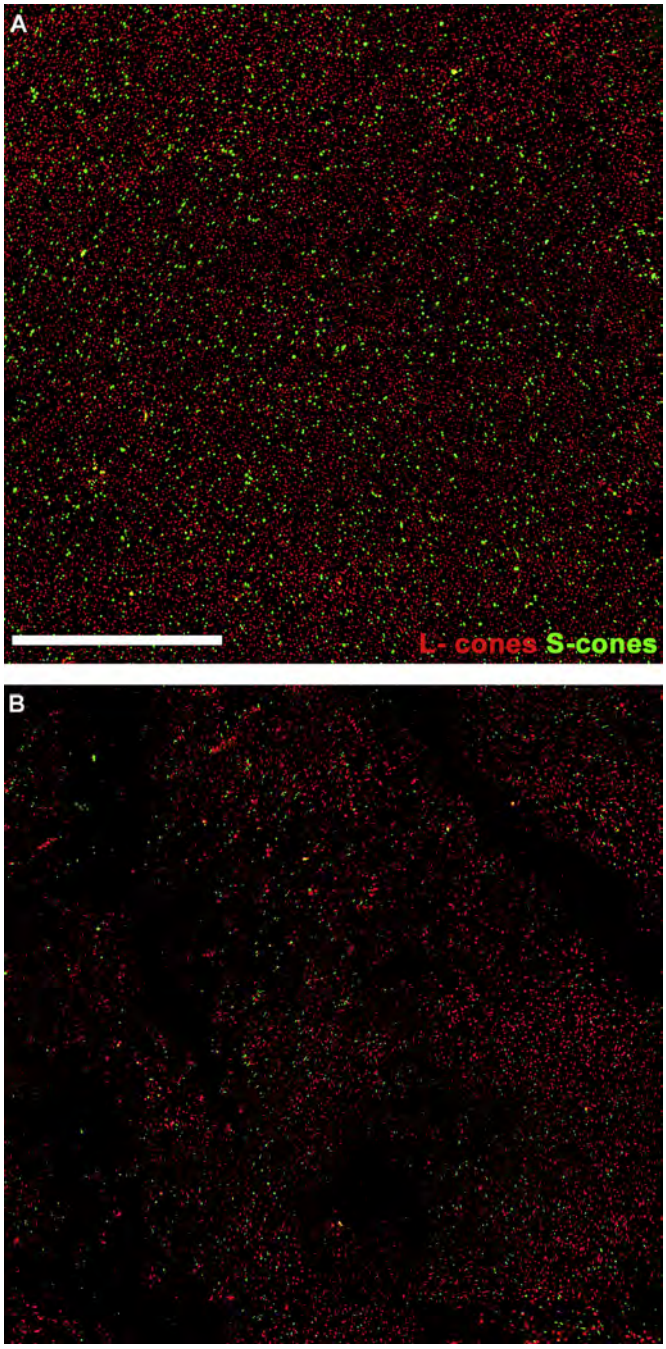

Fig. 11. Patchy loss of L- and S-cones in retinal whole-mounts. Micrographs from the inferior-nasal quadrant of a wholemounted right control (A) or a left experimental (B) retina analyzed 6 months after LP. In these merged images both types of cones (L-cones in red and S-cones in green) are observed and illustrate the normal appearance of cones (A) and their "patchy" areas lacking cone photoreceptors after OHT (B). Scale bar: 1 mm.

between the levels of cumulative IOP or the level of optic nerve damage with the loss of cone mRNA levels, but did find a correlation with eyes that had experienced higher IOP peaks short time before sacrifice; such finding was interpreted as an association between the decrease in cone opsin expression and IOP level. Moreover, the finding that some of the OHT-monkeys that failed to show high IOP peaks two weeks prior to sacrifice did not show diminished cone opsin expression suggested that cones could recover once IOP was reduced (Pelzel et al., 2006), this was strengthen by the presence in their in situ experiments of non-stained cells rather than the absence of cells, further suggesting that lack of cone opsin expression could be reversible. The under expression of rod and cone opsins observed in our experiments is in agreement with previous reports that have quantified mRNA expression in adult rats (Drouyer et al., 2008) and monkeys with experimental OHT and in humans eyes from glaucomatous donors

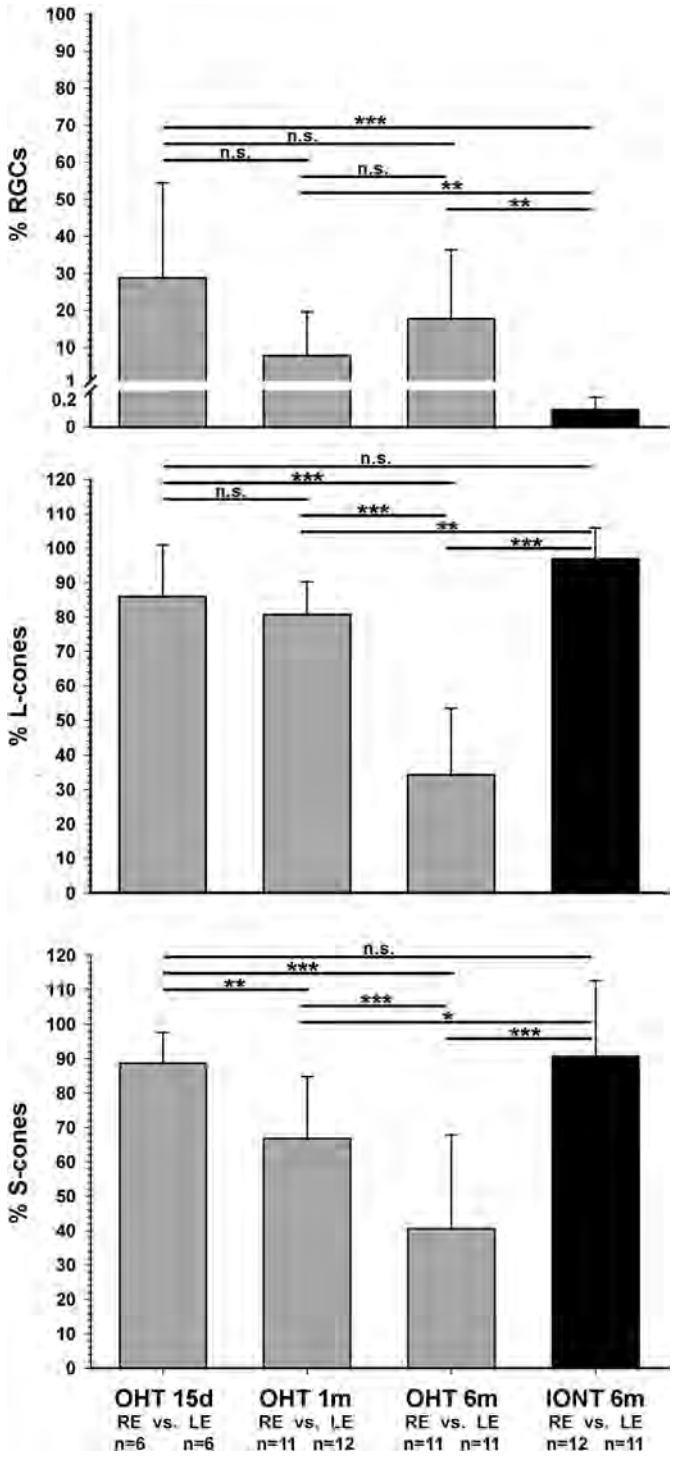

Fig. 12. Percentage of surviving RGCs, L-cones and S-cones after OHT and IONT. Histograms showing the mean percentage (±SD) of RGCs, L-cones, and S-cones (from top to bottom) 15 days, 1 and 6 months (m) after OHT (first, second and third columns) and 6 months after IONT (fourth column). T-test analysis, no significant differences (n.s.); $p < 0.05$ (*); $p < 0.01$ (**); $p < 0.001$ (***).

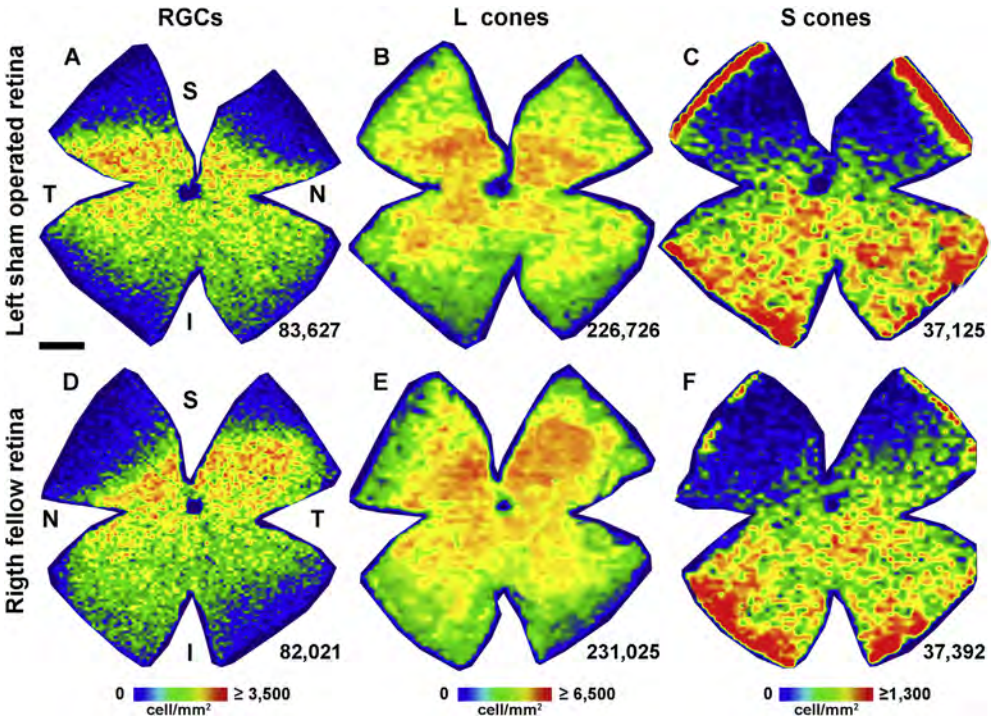

Fig. 13. Lasering the non-draining portion of the sclera does not lead to RGC, L- or S-cone loss. Isodensity maps showing the distribution of FG^{+}RGCs (A, D), L-cones (B, E) and S-cones (C, F) in a sham-operated left retina (A–C) and in their fellow non operated right retina (D–F). Bottom right of each map: number of RGCs, L- or S-cones counted in that retina. Density color scale is shown at the bottom of the image and ranges from 0 (purple) to 3500 or higher (red) RGCs/mm^2; to 6500 or higher (red) L-cones/mm^2, or to 1300 or higher (red) S cones/mm^2. S: superior, T temporal, I: inferior, N: nasal. Scale bar: 1 mm.

(Pelzel et al., 2006). In our experiments, we failed to find a significant correlation between cumulative IOP elevations as well as the IOP peaks observed during the first two weeks (when IOP elevations reach their maximum values) and the degree of RGC, L- or S-cone loss in every animal of the groups analyzed at 15 days and 1 or 6 months after LP-induced OHT. Moreover, our results, in contrast to those of Pelzel et al. (2006), do not show evidence for L- or S-cone recovery; we observed in retinal wholemounts patchy areas lacking both types of cone immunoreactive outer segments, which may well correspond to the focal regions of outer nuclear layer degeneration observed in the radially oriented paraffin embedded cross sections of the retina. In the latter, within the focal regions there were no cell nuclei in the ONL, indicating that in addition to L- and S-cones rods had also degenerated. Moreover, our results indicate that cone-photoreceptors degenerate insidiously and progressively; such degeneration is barely noticeable at 15 days (only for the S-cones) when most RGCs have lost their retrograde axonal transport capabilities, becomes apparent at 1 month when IOP levels return to normal, and reaches its maximum by 6 months after LP at a time when IOP had been at basal levels for five months. Thus, the time-course progression in our LP-induced OHT experiments indicates that the outer retinal pathology does not reverse when IOP returns to basal values but on the contrary continues progressing for long periods of time.

The protracted loss of L- and S-cones, together with the focal areas of ORL degeneration and the diminutions in the expression of the three opsins suggest a direct damage to the outer retina, independent from the RGC-axonal damage. It is possible that OHT triggers a slow developing degeneration that results six months later in severe functional and morphological alterations of the ORL with substantial degeneration of cones and rods. At present the type of injury leading to ORL degeneration is unknown, but one possible explanation is a transient ischemia of the choroid that could alter photoreceptor and/or pigment epithelial cell metabolism (Mayor-Torroglosa et al., 2005; Montalbán-Soler et al., 2012; García-Ayuso et al., 2013). Because in our experiments important IOP elevations were present during the first two weeks but decreased rapidly to basal levels by one month, it is possible that choroidal insufficiency may be a distinct pathological event. Indeed, decreased choroidal blood flow has been reported in monkeys with OHT (Alm and Bill, 1973) and in humans with GON (Kaiser et al., 1997).

Our results documenting protracted degeneration of the ORL are consistent with previous studies showing adverse effects on the outer retina affecting the cone photoreceptor population. This has been shown: i) in murine models analyzed functionally (Mittag et al., 2000; Salinas-Navarro et al., 2009a; Heiduschka et al., 2010; Georgiou et al., 2014; Pérez de Lara et al., 2014), anatomically (Guo et al., 2010; Fuchs et al., 2012; Fernández-Sánchez et al., 2014; Rojas et al., 2014) or both (Bayer et al., 2001; Cuenca et al., 2010; Calkins, 2012); ii) in monkey OHT models analyzed functionally (Liu et al., 2014) or anatomically (Nork, 2000; Nork et al., 2000), and; iii) in human GON analyzed with anatomical (Panda and Jonas, 1992; Nork, 2000; Nork et al., 2000; Lei et al., 2008; Werner et al., 2011; Choi et al., 2011) or functional examinations (Holopigian et al., 1990; Drasdo et al., 2001; Velten et al., 2001; Bessler et al., 2010; Kanis et al., 2010; Barboni et al., 2011; Werner et al., 2011). Thus photoreceptor loss, although not clearly recognized yet, may indeed constitute an important feature of the retinal pathology associated with increased levels of IOP and this may relate potentially to the human GONs.

Our present results, however, might appear to be at odds with previous studies not showing cone-photoreceptors loss in OHT human (Kendell et al., 1995) or monkey (Wygnanski et al., 1995) retinas. Several explanations may account for these discrepancies: i) our rat OHT-model share a number of typical characteristics of

acute angle-closure human glaucoma coursing with elevated IOP peaks (Vidal-Sanz et al., 2012). It is likely that the findings in the ORL of our study are mainly related to the elevated IOP, and these increments may mimic those observed in secondary angle-closure glaucoma reported to be associated with cone loss (Panda and Jonas, 1992; Nork, 2000; Nork et al., 2000; Calkins, 2012). Thus, it is possible that the levels of IOP reached in this model might have produced a choroidal insufficiency that results in a potentially exaggerated outer retinal pathology which constitutes a distinct feature of this model; ii) Variability in the results obtained in different murine (Levkovitch-Verbin et al., 2002; Mabuchi et al., 2003; Filippopoulos et al., 2006; Schlamp et al., 2006; Howell et al., 2007; Soto et al., 2008; Pérez de Lara et al., 2014) or monkey (Yücel et al., 2003) models of OHT may depend upon subtle differences in the methods employed to induce elevated-IOP, which in turn might result in different cumulative and peak IOP elevations (Levkovitch-Verbin et al., 2002; Mabuchi et al., 2003), as well as in different animal susceptibility; iii) To investigate cone-photoreceptor loss, rather than simply sampling areas of the retina, we have examined the entire retina in wholemounts instead of the central regions of the retina and focussed on the populations of L-and S-cones identified with specific antibodies (Ortín-Martínez et al., 2010), and; iv) These studies were undertaken long time after the original insult, analyzing the progression of the cone-loss between one and six months, well over five months after IOP had returned to basal levels.

4.3. The topology of cone-photoreceptor loss did not match RGC loss in the GCL

A comparison of the distribution of surviving RGCs and cone-photoreceptors after LP showed an overwhelming loss of RGCs compared to cone losses. There were regions of the retina lacking RGCs but not cone-photoreceptors and vice versa. Moreover, the geographical pattern of RGC loss was different from that of cones, while the former occurred mainly in triangular sectors the lack of cones was somewhat “patchy” and diffuse-like. In the IONT experiments, a different injury-induced RGC death model, the RGC population was, as expected (Villegas-Pérez et al., 1988, 1993), practically absent six months after intraorbital optic nerve section, and yet the cone population appeared normal. Taken together these results suggest that cone loss appears independent, but not necessarily completely unrelated to RGC loss (Nork, 2000).

4.4. Concluding remarks

In this study we have further investigated the effects of OHT-induced retinal damage in adult rats. In particular we have explored the degree and time course by which other non-RGC retinal neurons may be affected by OHT. The present rodent model of LP-induced OHT is not fully comparable to monkey or human GONs, but learning from rodent models may help understanding retinal or optic nerve damage in human GONs and designing new strategies to treat the disease or prevent its progression.

Our studies show that following OHT, the retina develops progressively an outer retinal pathology characterized by diminished expression of opsins, diminished numbers of L- and S-cone outer segments throughout the retina in a diffuse fashion together with the presence of patchy areas lacking both types of cone outer segments, the latter could well correspond to the focal areas of ORL degeneration observed in cross sections. Moreover, the geographical pattern of cone loss in these retinas appears independent of the RGC loss and advocates for an additional mechanism of damage to the retina. While some form of choroidal insufficiency might be responsible for the small focal areas of ORL degeneration, the diffuse protracted loss of cone outer segments may require additional studies to obtain further explanations.

Acknowledgments

We are grateful to Leticia Nieto-López for the technical contributions. Financial support for these studies was obtained from: Spanish Ministry of Economy and Competitiveness: SAF-2012-38328; ISCIII-FEDER “Una manera de hacer Europa” PI13/00643, PI13/01266, RETICS: RD12/0034/0014.

References

Agudo, M., Pérez-Marín, M.C., Lönngren, U., Sobrado, P., Conesa, A., Cánovas, I., Salinas-Navarro, M., Miralles-Imperial, J., Hallböök, F., Vidal-Sanz, M., 2008. Time course profiling of the retinal transcriptome after optic nerve transection and optic nerve crush. Mol. Vis. 14, 1050–1063.

Agudo, M., Pérez-Marín, M.C., Sobrado-Calvo, P., Lönngren, U., Salinas-Navarro, M., Cánovas, I., Nadal-Nicolás, F.M., Miralles-Imperial, J., Hallböök, F., Vidal-Sanz, M., 2009. Immediate upregulation of proteins belonging to different branches of the apoptotic cascade in the retina after optic nerve transection and optic nerve crush. Investig. Ophthalmol. Vis. Sci. 50, 424–431.

Alarcón-Martínez, L., de la Villa, P., Avilés-Trigueros, M., Blanco, R., Villegas-Pérez, M.P., Vidal-Sanz, M., 2009. Short and long term axotomy-induced ERG changes in albino and pigmented rats. Mol. Vis. 17, 2373–2383.

Alarcón-Martínez, L., Avilés-Trigueros, M., Galindo-Romero, C., Valiente-Soriano, J., Agudo-Barriuso, M., de la Villa, P., Villegas-Pérez, M.P., Vidal-Sanz, M., 2010. ERG changes in albino and pigmented mice after optic nerve transection. Vis. Res. 50, 2176–2187.

Alm, A., Bill, A., 1973. Ocular and optic nerve blood flow at normal and increased intraocular pressures in monkeys (*Macaca irus*): a study with radioactively labelled microspheres including flow determinations in brain and some other tissues. Exp. Eye Res. 15, 15–29.

Almasieh, M., Wilson, A.M., Morquette, B., Cueva Vargas, J.L., Di Polo, A., 2012. The molecular basis of retinal ganglion cell death in glaucoma. Prog. Retin. Eye Res. 31, 152–181.

Avilés-Trigueros, M., Sauvé, Y., Lund, R.D., Vidal-Sanz, M., 2000. Selective innervation of retinorecipient brainstem nuclei by retinal ganglion cell axons regenerating through peripheral nerve grafts in adult rats. J. Neurosci. 20, 361–374.

Avilés-Trigueros, M., Mayor-Torroglosa, S., García-Avilés, A., Lafuente, M.P., Rodríguez, M.E., Miralles de Imperial, J., Villegas-Pérez, M.P., Vidal-Sanz, M., 2003. Transient ischemia of the retina results in massive degeneration of the retinotectal projection: long-term neuroprotection with brimonidine. Exp. Neurol. 184, 767–777.

Barboni, M.T., Pangeni, G., Ventura, D.F., Horn, F., Kremers, J., 2011. Heterochromatic flicker electroretinograms reflecting luminance and cone opponent activity in glaucoma patients. Investig. Ophthalmol. Vis. Sci. 52, 6757–6765.

Bayer, A.U., Neuhardt, T., May, A.C., Martus, P., Maag, K.P., Brodie, S., Lütjen-Drecoll, E., Podos, S.M., Mittag, T., 2001. Retinal morphology and ERG response in the DBA/2NNia mouse model of angle-closure glaucoma. Investig. Ophthalmol. Vis. Sci. 42, 1258–1265.

Bessler, P., Klee, S., Kellner, U., Haueisen, J., 2010. Silent substitution stimulation of S-cone pathway and L- and M-cone pathway in glaucoma. Investig. Ophthalmol. Vis. Sci. 51, 319–326.

Bodeutsch, N., Siebert, H., Dermon, C., Thanos, S., 1999. Unilateral injury to the adult ratoptic nerve causes multiple cellular responses in the contralateral site. J. Neurobiol. 38, 116–128.

Burgoyne, C.F., Downs, J.C., Bellezza, A.J., Suh, J.K., Hart, R.T., 2005. The optic nerve head as a biomechanical structure: a new paradigm for understanding the role of IOP-related stress and strain in the pathophysiology of glaucomatous optic nerve head damage. Prog. Retin. Eye Res. 24, 39–73.

Calkins, D.J., 2012. Critical pathogenic events underlying progression of neurodegeneration in glaucoma. Prog. Retin. Eye Res. 31, 702–719.

Chidlow, G., Casson, R., Sobrado-Calvo, P., Vidal-Sanz, M., Osborne, N.N., 2005. Measurement of retinal injury in the rat after optic nerve transection: an RT-PCR study. Mol. Vis. 11, 387–396.

Choi, S.S., Zawadzki, R.J., Lim, M.C., Brandt, J.D., Keltner, J.L., Doble, N., Werner, J.S., 2011. Evidence of outer retinal changes in glaucoma patients as revealed by ultrahigh-resolution in vivo retinal imaging. Br. J. Ophthalmol. 95, 131–141.

Cone, F.E., Gelman, S.E., Son, J.L., Pease, M.E., Quigley, H.A., 2010. Differential susceptibility to experimental glaucoma among 3 mouse strains using bead and viscoelastic injection. Exp. Eye Res. 91, 415–424.

Cuenca, N., Pinilla, I., Fernández-Sánchez, L., Salinas-Navarro, M., Alarcón-Martínez, L., Avilés-Trigueros, M., de la Villa, P., Miralles de Imperial, J., Villegas-Pérez, M.P., Vidal-Sanz, M., 2010. Changes in the inner and outer retinal layers after acute increase of the intraocular pressure in adult albino Swiss mice. Exp. Eye Res. 91, 273–285.

de Hoz, R., Gallego, B.I., Ramírez, A.I., Rojas, B., Salazar, J.J., Valiente-Soriano, F.J., Avilés-Trigueros, M., Villegas-Perez, M.P., Vidal-Sanz, M., Triviño, A.,

Ramírez, J.M., 2013. Rod-like microglia are restricted to eyes with laser-induced ocular hypertension but absent from the microglial changes in the contralateral untreated eye. PLoS One 8, e83733.
Dekeyster, E., Aerts, J., Valiente-Soriano, F.J., De Groef, L., Salinas-Navarro, M., Vidal-Sanz, M., Arckens, L., Moons, L., 2015. Ocular hypertension results in retinotopic alterations in the visual cortex of adult mice. Curr. Eye Res. (in press).
Dijk, F., Kamphuis, W., 2004. An immunocytochemical study on specific amacrine cell subpopulations in the rat retina after ischemia. Brain Res. 1026, 205–217.
Drasdo, N., Aldebasi, Y.H., Chiti, Z., Mortlock, K.E., Morgan, J.E., North, R.V., 2001. The s-cone PHNR and pattern ERG in primary open angle glaucoma. Investig. Ophthalmol. Vis. Sci. 42, 1266–1272.
Drouyer, E., Dkhissi-Benyahya, O., Chiquet, C., WoldeMussie, E., Ruiz, G., Wheeler, L.A., Denis, P., Cooper, H.M., 2008. Glaucoma alters the circadian timing system. PLoS One 3, e3931.
Fernández-Sánchez, L., Pérez De Sevilla Müller, L., Brecha, N., Cuenca, N., 2014. Loss of outer retinal neurons and circuitry alterations in the DBA/2J mouse. Investig. Ophthalmol. Vis. Sci. 55, 6059–6072.
Filippopoulos, T., Danias, J., Chen, B., Podos, S.M., Mittag, T.W., 2006. Topographic and morphologic analyses of retinal ganglion cell loss in old DBA/2NNia mice. Investig. Ophthalmol. Vis. Sci. 47, 1968–1974.
Fuchs, M., Scholz, M., Sendelbeck, A., Atorf, J., Schlegel, C., Enz, R., Brandstätter, J.H., 2012. Rod photoreceptor ribbon synapses in DBA/2J mice show progressive age-related structural changes. PLoS One 7, e44645.
Gallego, B.I., Salazar, J.J., de Hoz, R., Rojas, B., Ramírez, A.I., Salinas-Navarro, M., Ortín-Martínez, A., Valiente-Soriano, F.J., Avilés-Trigueros, M., Villegas-Perez, M.P., Vidal-Sanz, M., Triviño, A., Ramírez, J.M., 2012. IOP induces upregulation of GFAP and MHC-II and microglia reactivity in mice retina contralateral to experimental glaucoma. J. Neuroinflammation 9, 92.
Galindo-Romero, C., Avilés-Trigueros, M., Jiménez-López, M., Valiente-Soriano, F.J., Salinas-Navarro, M., Nadal-Nicolás, F., Villegas-Pérez, M.P., Vidal-Sanz, M., Agudo-Barriuso, M., 2011. Axotomy-induced retinal ganglion cell death in adult mice: quantitative and topographic time course analyses. Exp. Eye Res. 92, 377–387.
García-Ayuso, D., Salinas-Navarro, M., Agudo, M., Cuenca, N., Pinilla, I., Vidal-Sanz, M., Villegas-Pérez, M.P., 2010. Retinal ganglion cell numbers and delayed retinal ganglion cell death in the P23H rat retina. Exp. Eye Res. 91, 800–810.
García-Ayuso, D., Ortín-Martínez, A., Jiménez-López, M., Galindo-Romero, C., Cuenca, N., Pinilla, I., Vidal-Sanz, M., Agudo-Barriuso, M., Villegas-Pérez, M.P., 2013. Changes in the photoreceptor mosaic of P23H-1 rats during retinal degeneration: implications for rod-cone dependent survival. Investig. Ophthalmol. Vis. Sci. 54, 5888–5900.
Garcia-Valenzuela, E., Shareef, S., Walsh, J., Sharma, S.C., 1995. Programmed cell death of retinal ganglion cells during experimental glaucoma. Exp. Eye Res. 61, 33–44.
Georgiou, A.L., Guo, L., Cordeiro, F.M., Salt, T.E., 2014. Electroretinogram and visual-evoked potential assessment of retinal and central visual function in a rat ocular hypertension model of glaucoma. Curr. Eye Res. 39, 472–486.
Guo, L., Normando, E.M., Nizari, S., Lara, D., Cordeiro, M.F., 2010. Tracking longitudinal retinal changes in experimental ocular hypertension using the cSLO and spectral domain-OCT. Investig. Ophthalmol. Vis. Sci. 51, 6504–6513.
Hayreh, S.S., 1969. Blood supply of the optic nerve head and its role in optic atrophy, glaucoma, and oedema of the optic disc. Br. J. Ophthalmol. 53, 721–748.
Heiduschka, P., Julien, S., Schuettauf, F., Schnichels, S., 2010. Loss of retinal function in aged DBA/2J mice – new insights into retinal neurodegeneration. Exp. Eye Res. 91, 779–783.
Holcombe, D.J., Lengefeld, N., Gole, G.A., Barnett, N.L., 2008. Selective inner retinal dysfunction precedes ganglion cell loss in a mouse glaucoma model. Br. J. Ophthalmol. 92, 683–688.
Holopigian, K., Seiple, W., Mayron, C., Koty, R., Lorenzo, M., 1990. Electrophysiological and psychophysical flicker sensitivity in patients with primary open-angle glaucoma and ocular hypertension. Investig. Ophthalmol. Vis. Sci. 31, 1863–1868.
Howell, G.R., Libby, R.T., Jakobs, T.C., Smith, R.S., Phalan, F.C., Barter, J.W., Barbay, J.M., Marchant, J.K., Mahesh, N., Porciatti, V., Whitmore, A.V., Masland, R.H., John, S.W., 2007. Axons of retinal ganglion cells are insulted in the optic nerve early in DBA/2J glaucoma. J. Cell Biol. 179, 1523–1537.
Huang, W., Fileta, J., Guo, Y., Grosskreutz, C.L., 2006. Downregulation of Thy1 in retinal ganglion cells in experimental glaucoma. Curr. Eye Res. 31, 265–271.
Jakobs, T.C., Libby, R.T., Ben, Y., John, S.W., Masland, R.H., 2005. Retinal ganglion cell degeneration is topological but not cell type specific in DBA/2J mice. J. Cell Biol. 171, 313–325.
Jia, L., Cepurna, W.O., Johnson, E.C., Morrison, J.C., 2000. Patterns of intraocular pressure elevation after aqueous humor outflow obstruction in rats. Investig. Ophthalmol. Vis. Sci. 41, 1380–1385.
Kaiser, H.J., Schoetzau, A., Stümpfig, D., Flammer, J., 1997. Blood-flow velocities of the extraocular vessels in patients with high-tension and normal-tension primary open-angle glaucoma. Am. J. Ophthalmol. 123, 320–327.
Kanis, M.J., Lemij, H.G., Berendschot, T.T., van de Kraats, J., van Norren, D., 2010. Foveal cone photoreceptor involvement in primary open-angle glaucoma. Graefes Arch. Clin. Exp. Ophthalmol. 248, 999–1006.
Kendell, K.R., Quigley, H.A., Kerrigan, L.A., Pease, M.E., Quigley, E.N., 1995. Primary open-angle glaucoma is not associated with photoreceptor loss. Investig. Ophthalmol. Vis. Sci. 36, 200–205.
Kielczewski, J.L., Pease, M.E., Quigley, H.A., 2005. The effect of experimental glaucoma and optic nerve transection on amacrine cells in the rat retina. Investig. Ophthalmol. Vis. Sci. 46, 3188–3196.
Kong, Y.X., Crowston, J.G., Vingrys, A.J., Trounce, I.A., Bui, V.B., 2009. Functional changes in the retina during and after acute intraocular pressure elevation in mice. Investig. Ophthalmol. Vis. Sci. 50, 5732–5740.
Korth, M., Nguyen, N.X., Jünemann, A., Martus, P., Jonas, J.B., 1994. VEP test of the blue-sensitive pathway in glaucoma. Investig. Ophthalmol. Vis. Sci. 35, 2599–2610.
Krishna, R., Mermoud, A., Baerveldt, G., Minckler, D.S., 1995. Circadian rhythm of intraocular pressure: a rat model. Ophthalmic Res. 27, 163–167.
Lafuente López-Herrera, M.P., Mayor-Torroglosa, S., Miralles de Imperial, J., Villegas-Pérez, M.P., Vidal-Sanz, M., 2002. Transient ischemia of the retina results in altered retrograde axoplasmic transport: neuroprotection with brimonidine. Exp. Neurol. 178, 243–258.
Lei, Y., Garrahan, N., Hermann, B., Becker, D.L., Hernandez, M.R., Boulton, M.E., Morgan, J.E., 2008. Quantification of retinal transneuronal degeneration in human glaucoma: a novel multiphoton-DAPI approach. Investig. Ophthalmol. Vis. Sci. 49, 1940–1945.
Levkovitch-Verbin, H., Quigley, H.A., Martin, K.R., Valenta, D., Baumrind, L.A., Pease, M.E., 2002. Translimbal laser photocoagulation to the trabecular meshwork as a model of glaucoma in rats. Investig. Ophthalmol. Vis. Sci. 43, 402–410.
Liu, K., Wang, N., Peng, X., Yang, D., Wang, C., Zeng, H., 2014. Long-term effect of laser-induced ocular hypertension on the cone electroretinogram and central macular thickness in monkeys. Photomed. Laser Surg. 32, 371–378.
Lönngren, U., Näpänkangas, U., Lafuente, M., Mayor, S., Lindqvist, N., Vidal-Sanz, M., Hallböök, F., 2006. The growth factor response in ischemic rat retina and superior colliculus after brimonidine pre-treatment. Brain Res. Bull. 71, 208–218.
Mabuchi, F., Aihara, M., Mackey, M.R., Lindsey, J.D., Weinreb, R.N., 2003. Optic nerve damage in experimental mouse ocular hypertension. Investig. Ophthalmol. Vis. Sci. 44, 4321–4330.
Mayor-Torroglosa, S., De la Villa, P., Rodríguez, M.E., López-Herrera, M.P., Avilés-Trigueros, M., García-Avilés, A., de Imperial, J.M., Villegas-Pérez, M.P., Vidal-Sanz, M., 2005. Ischemia results 3 months later in altered ERG, degeneration of inner layers, and deafferented tectum: neuroprotection with brimonidine. Investig. Ophthalmol. Vis. Sci. 46, 3825–3835.
Mittag, T.W., Danias, J., Pohorenec, G., Yuan, H.M., Burakgazi, E., Chalmers-Redman, R., Podos, S.M., Tatton, W.G., 2000. Retinal damage after 3 to 4 months of elevated intraocular pressure in a rat glaucoma model. Investig. Ophthalmol. Vis. Sci. 41, 3451–3459.
Montalbán-Soler, L., Alarcón-Martínez, L., Jiménez-López, M., Salinas-Navarro, M., Galindo-Romero, C., Bezerra de Sá, F., García-Ayuso, D., Avilés-Trigueros, M., Vidal-Sanz, M., Agudo-Barriuso, M., Villegas-Pérez, M.P., 2012. Retinal compensatory changes after light damage in albino mice. Mol. Vis. 18, 675–693.
Moon, J.I., Kim, I.B., Gwon, J.S., Park, M.H., Kang, T.H., Lim, E.J., Choi, K.R., Chun, M.H., 2005. Changes in retinal neuronal populations in the DBA/2J mouse. Cell. Tissue Res. 320, 51–59.
Moore, C.G., Johnson, E.C., Morrison, J.C., 1996. Circadian rhythm of intraocular pressure in the rat. Curr. Eye Res. 15, 185–191.
Morrison, J.C., Moore, C.G., Deppmeier, L.M., Gold, B.G., Meshul, C.K., Johnson, E.C., 1997. A rat model of chronic pressure-induced optic nerve damage. Exp. Eye Res. 64, 85–96.
Morrison, J.C., Johnson, E.C., Cepurna, W., Jia, L., 2005. Understanding mechanisms of pressure-induced optic nerve damage. Prog. Retin. Eye Res. 24, 217–240.
Morrison, J.C., Johnson, E., Cepurna, W.O., 2008. Rat models for glaucoma research. Prog. Brain Res. 173, 285–301.
Morrison, J.C., Cepurna Ying Guo, W.O., Johnson, E.C., 2011. Pathophysiology of human glaucomatous optic nerve damage: insights from rodent models of glaucoma. Exp. Eye Res. 93, 156–164.
Nadal-Nicolás, F.M., Jiménez-López, M., Sobrado-Calvo, P., Nieto-López, L., Cánovas-Martínez, I., Salinas-Navarro, M., Vidal-Sanz, M., Agudo, M., 2009. Brn3a as a marker of retinal ganglion cells: qualitative and quantitative time course studies in naive and optic nerve-injured retinas. Investig. Ophthalmol. Vis. Sci. 50, 3860–3868.
Nadal-Nicolás, F.M., Jiménez-López, M., Salinas-Navarro, M., Sobrado-Calvo, P., Alburquerque-Béjar, J.J., Vidal-Sanz, M., Agudo-Barriuso, M., 2012. Whole number, distribution and co-expression of brn3 transcription factors in retinal ganglion cells of adult albino and pigmented rats. PLoS One 7, e49830.
Nadal-Nicolás, F.M., Salinas-Navarro, M., Jiménez-López, M., Sobrado-Calvo, P., Villegas-Pérez, M.P., Vidal-Sanz, M., Agudo-Barriuso, M., 2014. Displaced retinal ganglion cells in albino and pigmented rats. Front. Neuroanat. 8, 99.
Nguyen, J.V., Soto, I., Kim, K.Y., Bushong, E.A., Oglesby, E., Valiente-Soriano, F.J., Yang, Z., Davis, C.H., Bedont, J.L., Son, J.L., Wei, J.O., Buchman, V.L., Zack, D.J., Vidal-Sanz, M., Ellisman, M.H., Marsh-Armstrong, N., 2011. Myelination transition zone astrocytes are constitutively phagocytic and have synuclein dependent reactivity in glaucoma. Proc. Natl. Acad. Sci. U. S. A. 108, 1176–1181.
Nork, T.M., 2000. Acquired color vision loss and a possible mechanism of ganglion cell death in glaucoma. Trans. Am. Ophthalmol. Soc. 98, 331–363.
Nork, T.M., Ver Hoeve, J.N., Poulsen, G.L., Nickells, R.W., Davis, M.D., Weber, A.J., Vaegan, Sarks, S.H., Lemley, H.L., Millecchia, L.L., 2000. Swelling and loss of photoreceptors in chronic human and experimental glaucomas. Arch. Ophthalmol. 118, 235–245.
Ortín-Martínez, A., Jiménez-López, M., Nadal-Nicolás, F.M., Salinas-Navarro, M., Alarcón-Martínez, L., Sauvé, Y., Villegas-Pérez, M.P., Vidal-Sanz, M., Agudo-Barriuso, M., 2010. Automated quantification and topographical distribution of the whole population of S- and L-cones in adult albino and pigmented rats.

Investig. Ophthalmol. Vis. Sci. 51, 3171–3183.
Ortín-Martínez, A., et al., 2012. IOVS 53 (ARVO E-Abstract 2488).
Ortín-Martínez, A., Nadal-Nicolás1, F.M., Jiménez-López, M., Alburquerque-Béjar, J.J., Nieto-López, L., García-Ayuso, D., Villegas-Pérez, M.P., Vidal-Sanz, M., Agudo-Barriuso, M., 2014. Number and distribution of mouse retinal cone photoreceptors: differences between an albino (Swiss) and a pigmented (C57/BL6) strain. PLoS One 9, e102392.
Panda, S., Jonas, J.B., 1992. Decreased photoreceptor count in human eyes with secondary angle-closure glaucoma. Investig. Ophthalmol. Vis. Sci. 33, 2532–2536.
Parrilla-Reverter, G., Agudo, M., Nadal-Nicolás, F., Alarcón-Martínez, L., Jiménez-López, M., Salinas-Navarro, M., Sobrado-Calvo, P., Bernal-Garro, J.M., Villegas-Pérez, M.P., Vidal-Sanz, M., 2009. Time-course of the retinal nerve fibre layer degeneration after complete intra-orbital optic nerve transection or crush: a comparative study. Vis. Res. 49, 2808–2825.
Pelzel, H.R., Schlamp, C.L., Poulsen, G.L., Ver Hoeve, J.A., Nork, T.M., Nickells, R.W., 2006. Decrease of cone opsin mRNA in experimental ocular hypertension. Mol. Vis. 26, 1272–1282.
Pelzel, H.R., Schlamp, C.L., Waclawski, M., Shaw, M.K., Nickells, R.W., 2012. Silencing of Fem1cR3 gene expression in the DBA/2J mouse precedes retinal ganglion cell death and is associated with histone deacetylase activity. Investig. Ophthalmol. Vis. Sci. 53, 1428–1435.
Pérez de Lara, M.J., Santano, C., Guzmán-Aránguez, A., Valiente-Soriano, F.J., Avilés-Trigueros, M., Vidal-Sanz, M., de la Villa, P., Pintor, J., 2014. Assessment of inner retina dysfunction and progressive ganglion cell loss in a mouse model of glaucoma. Exp. Eye Res. 122, 40–49.
Perry, V.H., Cowey, A., 1979. The effects of unilateral cortical and tectal lesions on retinal ganglion cells in rats. Exp. Brain Res. 35, 85–95.
Perry, V.H., 1981. Evidence for an amacrine cell system in the ganglion cell layer of the rat retina. Neuroscience 6, 931–944.
Quigley, H.A., Green, W.R., 1979. The histology of human glaucoma cupping and optic nerve damage: clinicopathologic correlation in 21 eyes. Ophthalmology 86, 1803–1830.
Quigley, H.A., Hohman, R.M., 1983. Laser energy levels for trabecular meshwork damage in the primate eye. Investig. Ophthalmol. Vis. Sci. 24, 1305–1307.
Quigley, H.A., 1999. Neuronal death in glaucoma. Prog. Retin. Eye Res. 18, 39–57.
Ramírez, A.I., Salazar, J.J., de Hoz, R., Rojas, B., Gallego, B.I., Salinas-Navarro, M., Alarcón-Martínez, L., Ortín-Martínez, A., Avilés-Trigueros, M., Vidal-Sanz, M., Triviño, A., Ramírez, J.M., 2010. Quantification of the effect of different levels of IOP in the astroglia of the rat retina ipsilateral and contralateral to experimental glaucoma. Investig. Ophthalmol. Vis. Sci. 51, 5690–5696.
Rasband, W.S., 1997–2014. ImageJ. U. S. National Institutes of Health, Bethesda, MD, USA. http://imagej.nih.gov/ij/.
Rojas, B., Gallego, B.I., Ramirez, A.I., Salazar, J.J., de Hoz, R., Valiente-Soriano, F.J., Avilés-Trigueros, M., Villegas-Perez, M.P., Vidal-Sanz, M., Triviño, A., Ramirez, J.M., 2014. Microglia in mice retina contralateral to experimental glaucoma exhibit multiple signs of activation in all retinal layers. J. Neuroinflammation 11, 133.
Salinas-Navarro, M., Alarcón-Martínez, L., Valiente-Soriano, F.J., Ortín-Martínez, A., Jiménez-López, M., Avilés-Trigueros, M., Villegas-Pérez, M.P., de la Villa, P., Vidal-Sanz, M., 2009a. Functional and morphological effects of laser-induced ocular hypertension in retinas of adult albino Swiss mice. Mol. Vis. 15, 2578–2598.
Salinas-Navarro, M., Mayor-Torroglosa, S., Jiménez-López, M., Avilés-Trigueros, M., Holmes, T.M., Lund, R.D., Villegas-Pérez, M.P., Vidal-Sanz, M., 2009b. A computerized analysis of the entire retinal ganglion cell population and its spatial distribution in adult rats. Vis. Res. 49, 115–126.
Salinas-Navarro, M., Alarcón-Martínez, L., Valiente-Soriano, F.J., Jiménez-López, M., Mayor-Torroglosa, S., Avilés-Trigueros, M., Villegas-Pérez, M.P., Vidal-Sanz, M., 2010. Ocular hypertension impairs optic nerve axonal transport leading to progressive retinal ganglion cell degeneration. Exp. Eye Res. 90, 168–183.
Salinas-Navarro, M., et al., 2011. IOVS 52 (ARVO E-Abstract. 2459).
Sánchez-Migallón, M.C., Nadal-Nicolás, F.M., Jiménez-López, M., Sobrado-Calvo, P., Vidal-Sanz, M., Agudo-Barriuso, M., 2011. Brain derived neurotrophic factor maintains Brn3a expression in axotomized rat retinal ganglion cells. Exp. Eye Res. 92, 260–267.
Sappington, R.M., Carlson, B.J., Crish, S.D., Calkins, D.J., 2010. The microbead occlusion model: a paradigm for induced ocular hypertension in rats and mice. Investig. Ophthalmol. Vis. Sci. 51, 207–216.
Savini, G., Carbonelli, M., Barboni, P., 2011. Spectral-domain optical coherence tomography for the diagnosis and follow-up of glaucoma. Curr. Opin. Ophthalmol. 22, 115–123.
Savini, G., Barboni, P., Carbonelli, M., Sbreglia, A., Deluigi, G., Parisi, V., 2013. Comparison of optic nerve head parameter measurements obtained by time-domain and spectral-domain optical coherence tomography. J. Glaucoma 22, 384–389.
Schlamp, C.L., Johnson, E.C., Li, Y., Morrison, J.C., Nickells, R.W., 2001. Changes in Thy1 gene expression associated with damaged retinal ganglion cells. Mol. Vis. 7, 192–201.
Schlamp, C.L., Li, Y., Dietz, J.A., Janssen, K.T., Nickells, R.W., 2006. Progressive ganglion cell loss and optic nerve degeneration in DBA/2J mice is variable and asymmetric. BMC Neurosci. 7, 66.
Schlamp, C.L., Montgomery, A.D., Mac Nair, C.E., Schuart, C., Willmer, D.J., Nickells, R.W., 2013. Evaluation of the percentage of ganglion cells in the ganglion cell layer of the rodent retina. Mol. Vis. 19, 1387–1396.
Schnebelen, C., Pasquis, B., Salinas-Navarro, M., Joffre, C., Creuzot-Garcher, C.P., Vidal-Sanz, M., Bron, A.M., Bretillon, L., Acar, N., 2009. A dietary combination of omega-3 and omega-6 polyunsaturated fatty acids is more efficient than single supplementations in the prevention of retinal damage induced by elevation of intraocular pressure in rats. Graefes Arch. Clin. Exp. Ophthalmol. 247, 1191–1203.
Sellés-Navarro, I., Villegas-Pérez, M.P., Salvador-Silva, M., Ruiz-Gómez, J.M., Vidal-Sanz, M., 1996. Retinal ganglion cell death after different transient periods of pressure-induced ischemia and survival intervals. A quantitative in vivo study. Investig. Ophthalmol. Vis. Sci. 37, 2002–2014.
Sobrado-Calvo, P., Vidal-Sanz, M., Villegas-Pérez, M.P., 2007. Rat retinal microglial cells under normal conditions, after optic nerve section, and after optic nerve section and intravitreal injection of trophic factors or macrophage inhibitory factor. J. Comp. Neurol. 501, 866–878.
Soto, I., Oglesby, E., Buckingham, B.P., Son, J.L., Roberson, E.D., Steele, M.R., Inman, D.M., Vetter, M.L., Horner, P.J., Marsh-Armstrong, N., 2008. Retinal ganglion cells downregulate gene expression and lose their axons within the optic nerve head in a mouse glaucoma model. J. Neurosci. 28, 548–561.
The AGIS investigators, 2000. The Advanced Glaucoma Intervention Study (AGIS): 7. The relationship between control of intraocular pressure and visual field deterioration. The AGIS investigators. Am. J. Ophthalmol. 130, 429–440.
Velten, I.M., Korth, M., Horn, F.K., 2001. The a-wave of the dark adapted electroretinogram in glaucomas: are photoreceptors affected? Br. J. Ophthalmol. 85, 397–402.
Vidal-Sanz, M., Lafuente, M., Sobrado-Calvo, P., Selles-Navarro, I., Rodriguez, E., Mayor-Torroglosa, S., Villegas-Perez, M.P., 2000. Death and neuroprotection of retinal ganglion cells after different types of injury. Neurotox. Res. 2, 215–227.
Vidal-Sanz, M., Avilés-Trigueros, M., Whiteley, S.J., Sauvé, Y., Lund, R.D., 2002. Reinnervation of the pretectum in adult rats by regenerated retinal ganglion cell axons: anatomical and functional studies. Prog. Brain Res. 137, 443–452.
Vidal-Sanz, M., de la Villa, P., Avilés-Trigueros, M., Mayor-Torroglosa, S., Salinas-Navarro, M., Alarcón-Martínez, L., Villegas-Pérez, M.P., 2007. Neuroprotection of retinal ganglion cell function and their central nervous system targets. Eye 21, S42–S45.
Vidal-Sanz, M., Salinas-Navarro, M., Nadal-Nicolás, F.M., Alarcón-Martínez, L., Valiente-Soriano, F.J., de Imperial, J.M., Avilés-Trigueros, M., Agudo-Barriuso, M., Villegas-Pérez, M.P., 2012. Understanding glaucomatous damage: anatomical and functional data from ocular hypertensive rodent retinas. Prog. Retin. Eye Res. 31, 1–27.
Villegas-Pérez, M.P., Vidal-Sanz, M., Bray, G.M., Aguayo, A.J., 1988. Influences of peripheral nerve grafts on the survival and regrowth of axotomized retinal ganglion cells in adult rats. J. Neurosci. 8, 265–280.
Villegas-Pérez, M.P., Vidal-Sanz, M., Rasminsky, M., Bray, G.M., Aguayo, A.J., 1993. Rapid and protracted phases of retinal ganglion cell loss follow axotomy in the optic nerve of adult rats. J. Neurobiol. 24, 23–36.
Weishaupt, J.H., Klocker, N., Bahr, M., 2005. Axotomy-induced early down-regulation of POU-IV class transcription factors Brn-3a and Brn-3b in retinal ganglion cells. J. Mol. Neurosci. 26, 17–25.
Werner, J.S., Keltner, J.L., Zawadzki, R.J., Choi, S.S., 2011. Outer retinal abnormalities associated with inner retinal pathology in nonglaucomatous and glaucomatous optic neuropathies. Eye 25, 279–289.
WoldeMussie, E., Ruiz, G., Wijono, M., Wheeler, L.A., 2001. Neuroprotection of retinal ganglion cells by brimonidine in rats with laser-induced chronic ocular hypertension. Investig. Ophthalmol. Vis. Sci. 42, 2849–2855.
Wygnanski, T., Desatnik, H., Quigley, H.A., Glovinsky, Y., 1995. Comparison of ganglion cell loss and cone loss in experimental glaucoma. Am. J. Ophthalmol. 120, 184–189.
Yücel, Y.H., Zhang, Q., Weinreb, R.N., Kaufman, P.L., Gupta, N., 2003. Effects of retinal ganglion cell loss on magno-, parvo-, koniocellular pathways in the lateral geniculate nucleus and visual cortex in glaucoma. Prog. Retin. Eye Res. 22, 465–481.